

①

Semi-Annual Technical Report
1 October 1976 to 31 March 1977

ARPA Order No.: 3291
Program Code: 7F10
Contractor: Saint Louis University
Effective Date of Contract: 1 March 1973
Contract Expiration Date: 30 September 1977
Amount of Contract: \$211,459
Contract Number: F44620-73-C-0042
Principal Investigators: Brian J. Mitchell
Otto W. Nuttli
Phone: 314-535-3300, Ext. 547
Program Manager: Brian J. Mitchell
Short Title: Research in Seismology ✓

DTIC
ELECTE
NOV 1 1982
H

APPROVED FOR PUBLIC RELEASE
DISTRIBUTION UNLIMITED

Sponsored by

Advanced Research Projects Agency (DOD)

ARPA Order No. 3291

Monitored by AFOSR Under Contract #F44620-73-C-0042

The views and conclusions contained in this document are those of the authors and should not be interpreted as necessarily representing the official policies, either expressed or implied, of the Defense Advanced Research Projects Agency or the U.S. Government.

82 11 01 224

ADA 120894

DTIC FILE COPY

Research in Seismology
Semi-Annual Technical Report
Contract F44620-73-C-0042

Table of Contents

Technical Report Summary	Page 2
Work Completed During the Report Period	
Introduction	4
The Scaling of Teleseismic P-wave Ground-Motion Spectra of Underground Nuclear Explosions	5
Love Waves as an Explosion-Earthquake Discriminant	27
Modelling Complex Earthquakes	72
The Effect of Complex Near-Source Crustal Structure on the Wave Forms of Rayleigh Waves	78

Accession For	
NTIS GRA&I	<input checked="" type="checkbox"/>
DTIC TAB	<input type="checkbox"/>
Unannounced	<input type="checkbox"/>
Justification	
By _____	
Distribution/	
Availability Codes	
Dist	Avail and/or Special



Technical Report Summary

P-wave ground motion spectra at teleseismic distances have been obtained for several nuclear events. These include several events in tuff and rhyolite, and one in granite, at NTS, several USSR events at the Kazakh test region, and one event in the Aleutians. The observed spectra for these events were compared to theoretically expected spectra for a nuclear explosion source. m_b values have been found to scale as the 1-sec P-wave spectral amplitudes at both NTS and Kazakh. Similarly, M_s values scale as the 20-sec P-wave spectral amplitudes, except in the case of one NTS event (BOXCAR) which had anomalously large surface waves. At long periods, events with similar M_s values at NTS and Kazakh have similar spectral levels. At shorter periods (near 1 sec), however, the Kazakh events had a higher spectral level than events at NTS. This probably indicates that the anelastic attenuation is greater beneath NTS than beneath the Kazakh region. However, 1-sec spectral levels for PILEDRIVER, which occurred in granite at NTS, are somewhat higher than those for events in tuff or rhyolite. Consequently, the shot medium as well as the Q structure appear to affect the spectra at short periods. The amplitudes of 1-sec P-waves for Aleutian explosions depend on azimuth, apparently because of focussing and defocussing due to the subducting Pacific plate.

Love waves were used to study nine Eurasian events which were anomalous by the $m_b:M_s$ criterion (using Rayleigh waves for M_s). The number of anomalous events was reduced to six with the $m_b:M_s$ criterion if Love waves

were used to determine M_s . If the Love wave amplitude spectrum is used, only four of the earthquakes were found to be anomalous.

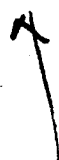
Complex rupture processes are being studied by comparing observed teleseismic P-waves on long-period records to those obtained by computing theoretical seismograms using the Haskell-Thomson method. Two events were selected which occurred in a region of well known crust and upper mantle structure. The P-wave for one event can be synthesized very well with a simple rupture process (a single event) whereas the other event appears to consist of two or more separate ruptures.

Observed Rayleigh waves from earthquakes with known fault-plane solutions have been compared to theoretical Rayleigh wave seismograms in an attempt to assess the effects of propagation path and near-source complexities on the wave forms of Rayleigh waves. For earthquakes which occur in the transition region between the stable crust of northern Asia and the Himalayas, variations in near source structure do not appear to have a great effect on the gross features of Rayleigh wave forms. Minor departures from theoretically expected wave-forms occur in almost all cases, but it is difficult to separate the effects of near-source complexities from those of multi-pathing or departures from an idealized source geometry. Observed Rayleigh wave forms for an event on Novaya Zemlya differ greatly from those for expected synthetic seismograms. This could be due to complex near-source structure, the presence of a portion of oceanic path near the source, or a source spectrum which differs greatly from that which would be expected from presently accepted models for nuclear explosions.



INTRODUCTION

Research for this report period has been concerned with the effect which various propagation effects and source properties have on the spectra and wave forms of body- and surface-waves. The research is divided into four different but related reports which are presented in the following sections. The first report, by Otto W. Nuttli and John A. Wagner is concerned with the scaling of teleseismic P-wave ground-motion spectra of underground nuclear explosions. The second, by Huei-Yuin Wen describes the use of Love waves as an explosion-earthquake discriminant. The third, by Jaime Yamamoto, describes a method for modelling complex earthquakes and presents comparisons with observed data. The fourth, by Brian J. Mitchell and Chiung-Chuan Cheng, reports work on assessing the effect of complex near-source structure on the wave forms of Rayleigh waves.



THE SCALING OF TELESEISMIC P-WAVE GROUND-MOTION
SPECTRA OF UNDERGROUND NUCLEAR EXPLOSIONS

by

Otto W. Nuttli and John A. Wagner

Introduction

Body-wave, m_b , and surface-wave, M_S , magnitudes of underground nuclear explosions have been used to discriminate them from earthquakes and to estimate their yield. To arrive at m_b and M_S values, amplitude measurements are made in the time domain at periods of 1 and 20 sec, respectively. Spectral measurements, on the other hand, provide amplitude information over a broad range of frequencies rather than at two discrete points and thus potentially carry more information. Furthermore, the explosion spectra may be thought of as the limiting case of earthquake spectra for earthquakes having a small source volume and time duration, and thus the scaling of explosion spectra should provide a limit for earthquake spectral scaling, about which much remains to be learned.

This report is concerned with an investigation of the teleseismic P-wave ground motion spectra of explosion-generated waves. We intend to follow it up with an investigation of the spectra of earthquakes, including those which are considered anomalous and non-anomalous by the $m_b:M_S$ criterion, to see in what ways explosion and earthquake P-wave ground-motion spectra differ from each other.

Far-Field Spectra

Murphy (1977) has presented far-field P-wave displacement spectra as a function of yield for underground nuclear explosions in saturated

tuff, for what he calls his modified source model. These spectra do not take account of anelastic attenuation, whose effect is to make the spectra drop off more rapidly at the shorter periods. Figure 1 shows the P-wave ground-motion spectra at a distance of 30° based on Murphy's (1977) modified source model and three assumed values of the Futterman (1962) attenuation operator T/Q (T is travel time and Q is the quality factor). For teleseismic P waves Carpenter (1967) found $T/Q = 1.1$ and Helmberger (1973) obtained $T/Q = 1.0$. Plotted in Figure 1 are spectra for $T/Q = 1.0$, 0.55 and 0, the latter corresponding to the curves presented by Murphy (1977). Note from the figure that the effect of decreasing Q is to make the spectral curves fall off more rapidly at the shorter periods. For example, at a period of 1 sec the spectral amplitude for $T/Q = 1.0$ is more than an order of magnitude less than that for $T/Q = 0$. Because body-wave magnitude, m_b , is obtained from amplitude measurements near 1-sec period, it should be very sensitive to the amount of absorption. Also, for a given yield the "corner period" increases as the value of T/Q increases. For the curves $T/Q = 0.55$ and 1.0 the "corner period" is taken to be the period at which the asymptotes for the short-period and long-period portions of the spectral curve intersect.

Murphy (1977) used relative amplitudes for the far-field P-wave spectra. The absolute amplitudes given on the ordinate axis in Figure 1 were determined from P-wave spectra of NTS events of known yield which were recorded at a distance of 30° . These spectra are given in Figure 2.

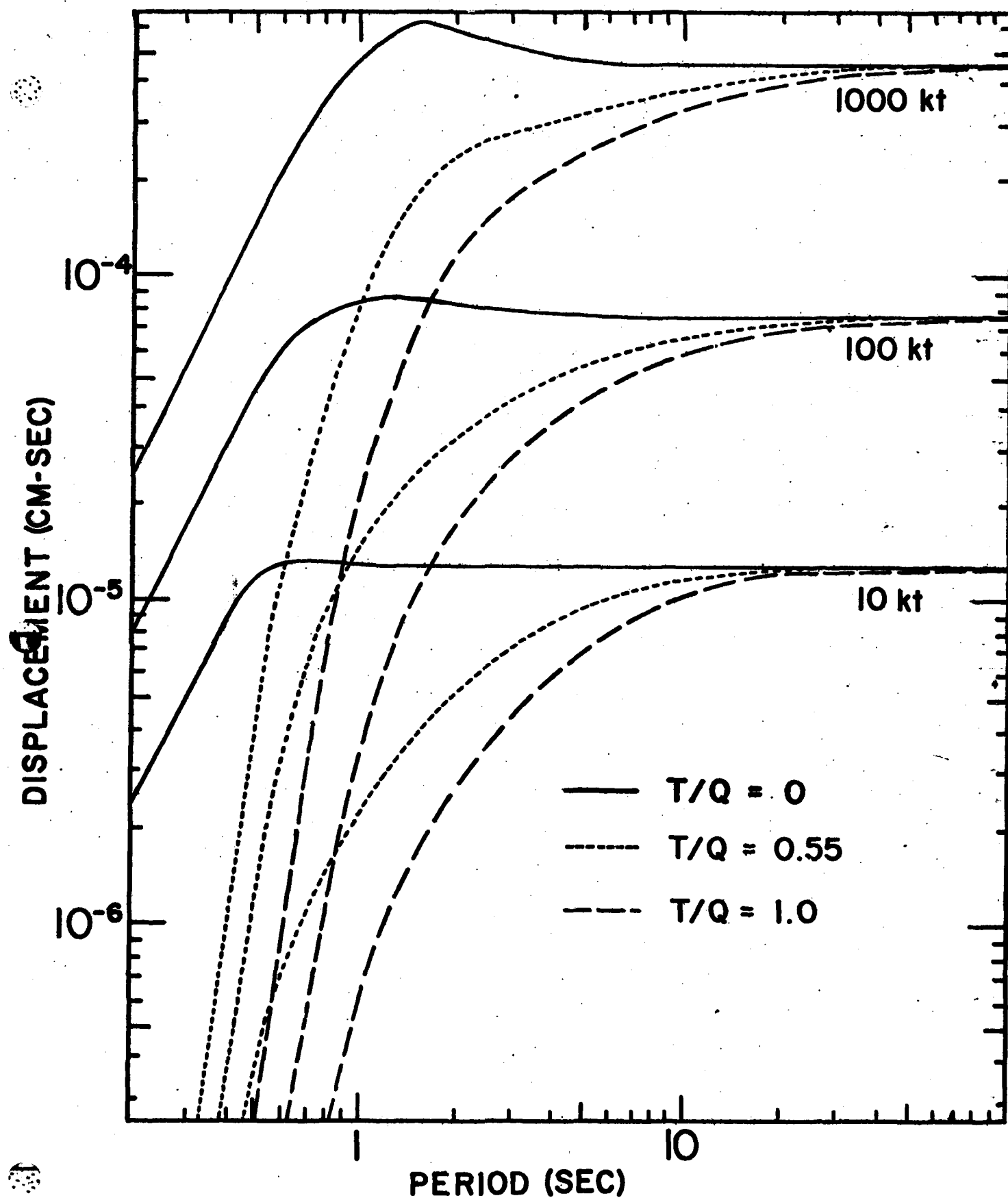


Figure 1. Theoretical P-wave ground-motion spectra at 30° for Murphy's (1977) modified source model. The quantity T/Q is the Futterman (1962) attenuation operator.

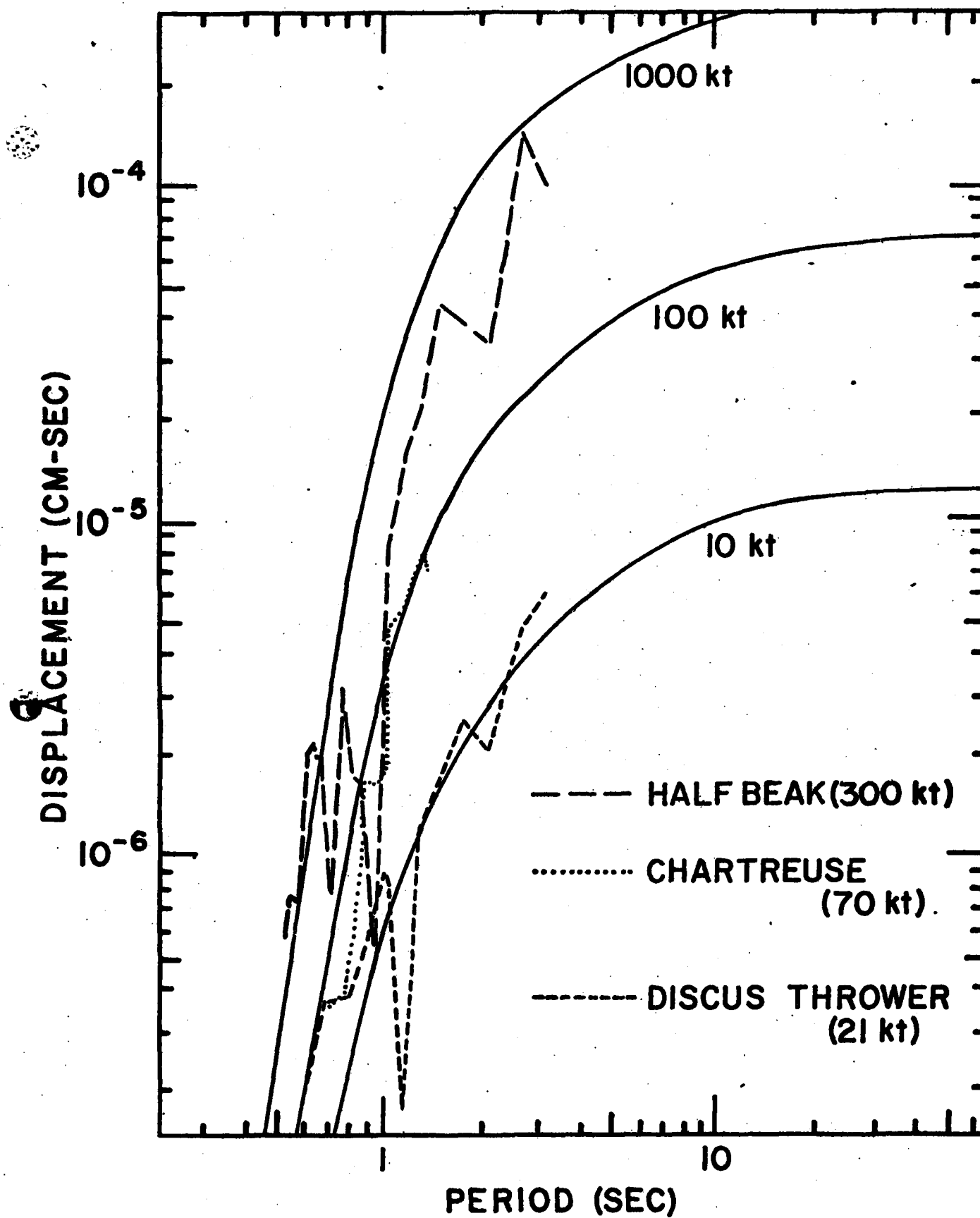


Figure 2. Theoretical P-wave ground-motion spectra at 30° for $T/Q = 1.0$ and observed spectra from short-period seismograms at 30° for 3 NTS explosions.

P-Wave Ground-Motion Spectra From NTS Events

Springer and Kinneman (1971) have given yields of some NTS events. Of them we have selected HALF BEAK (300 kt), CHARTREUSE (70 kt) and DISCUS THROWER (21 kt) to compare their P-wave ground-motion spectra at a distance of 30° with those predicted by Murphy's (1977) modified source model. The HALF BEAK spectrum is of the P-wave motion recorded at SCP (Pennsylvania) at a distance of 30° . The CHARTREUSE and DISCUS THROWER spectra are of the P-wave ground motion recorded at COL (Alaska) at a distance of 33° . We found that at their short-period end the spectra fall off in a manner closest to that of the theoretical $T/Q = 1.0$ curve. In Figure 2 we show the plot of the three single-station spectra (dashed lines) and the theoretical curves of Murphy's model for $T/Q = 1.0$. The observed spectra were obtained from the short-period seismograms after correction for instrument response. The digitizing interval was 0.17 sec and the length of the P-wave motion sampled was 20 sec. The response of the short-period seismograph system limits the reliable values of the spectra to the period range of about 0.5 to 2 or 3 sec.

Figure 3 contains smoothed P-wave ground-motion spectra at an epicentral distance of 30° for 8 NTS events detonated in tuff and rhyolite. Table 1 identifies the numbered events. All the spectra except those of HALF BEAK and BOXCAR were obtained from the COL seismograms at a distance of 33° . The short-period part of the BOXCAR spectrum was obtained from the NNA (Peru) short-period seismogram at a distance of 62° , which was normalized to a distance of 30° using the curve of Langston and Helmberger (1975). A portion of the BOXCAR spectrum between periods of 3 to 5 sec was obtained from the long-period seismogram of OGD (New Jersey), which is at a distance of 32° . The HALF BEAK spectrum, as noted previously, was obtained from

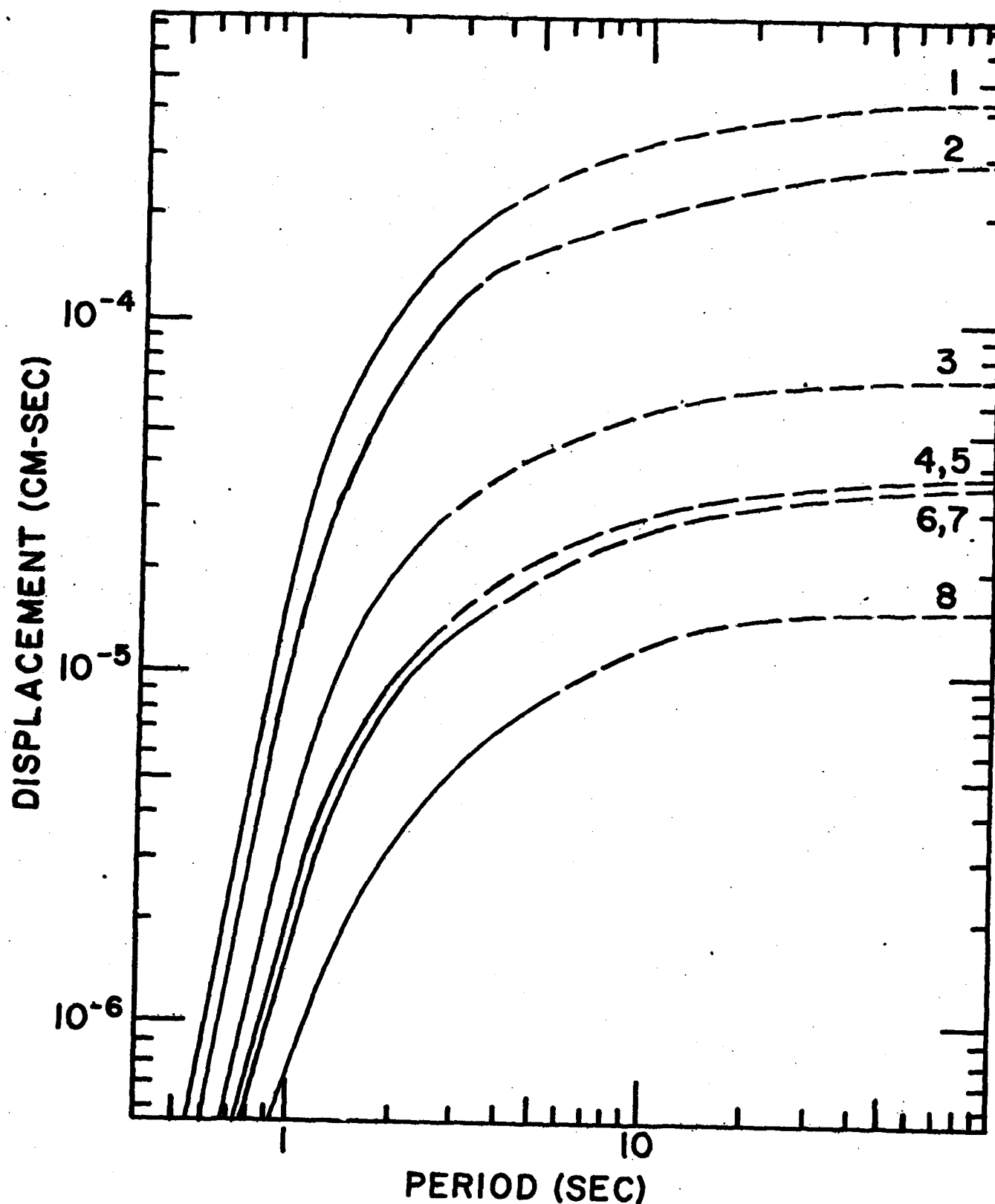


Figure 3. Smoothed P-wave ground-motion spectra normalized to 30° for selected NTS events. The dashed-line portions of the spectra indicate extrapolations based on Murphy's (1977) modified source model. The events corresponding to the numbers are identified in Table 1.

TABLE 1
SOURCE PARAMETERS OF SELECTED NTS EVENTS

Number	Name	Date	m_b	M_S	
1	BOXCAR	Apr. 26, 68	6.2	5.47 ± 0.22	(51)
2	HALF BEAK	Jun. 30, 66	6.1	4.86	0.18 (48)
3	ZAZA	Sep. 27, 67	5.7	4.12	0.28 (14)
4	BRONZE	Jul. 23, 65	5.4	3.60	0.15 (14)
5	DURVEA	Apr. 14, 66	5.4	3.72	(2)
6	CHARTREUSE	May 06, 66	5.4	3.70	0.23 (8)
7	CUP	Mar, 26, 65	--	3.86	0.16 (4)
8	DISCUS THROWER	May 27, 66	5.0	3.16	(2)

the long-period seismogram of OGD (New Jersey), which is at a distance of 32° . The HALF BEAK spectrum, as noted previously, was obtained from the SCP short-period seismogram. All the spectra of Figure 3 were smoothed, using as a guide the Murphy curves for $T/Q = 1.0$. The dashed portions of the spectra indicate extrapolations based on Murphy's curves.

Values of the body-wave magnitude, m_b , and the surface-wave magnitude, M_S , of the 8 events of Figure 3 are given in Table 1. The m_b values were taken from the publications of the International Seismological Centre. The M_S values were determined by us, using the amplitudes of the vertical-component Rayleigh-wave motion at 20-sec period. The number in parentheses following the M_S value indicates the number of stations used in the M_S determination. The number following the \pm sign is the standard deviation of the average M_S value.

We can observe from Table 1 and Figure 3 that all the spectral levels increase as m_b increases, i.e. the larger the m_b value, the larger the spectral amplitude. In a more quantitative sense, we can compare changes in m_b with changes in the logarithm of the spectral level at 1-sec period. The results are given in Table 2, in which all events are compared to BOXCAR (event no. 1). In all cases except CHARTREUSE, the difference between Δm_b and $\Delta \log_{10} A(1 \text{ sec})$ is only 0.1 unit. For CHARTREUSE it is 0.2 units. This is truly remarkable, for the uncertainties in both the smoothed spectral amplitudes and the m_b values are at least 0.2 units each. It indicates that in spite of the fact that the P-wave displacement spectrum is falling off rapidly at periods near 1 sec, the m_b value is a good estimate of the spectral amplitude at 1-sec period.

TABLE 2
DIFFERENCES IN m_b AND $\log_{10} A(1 \text{ sec})$ FOR
SELECTED EVENTS, COMPARED TO BOXCAR

Number	Name	Δm_b	$\Delta \log_{10} A(1 \text{ sec})$
1	BOXCAR	--	--
2	HALF BEAK	0.1	0.2
3	ZAZA	0.5	0.6
4	BRONZE	0.8	0.9
5	DURYEA	0.8	0.9
6	CHARTREUSE	0.8	1.0
7	CUP	--	1.0
8	DISCUS THROWER	1.2	1.3

We can also see how the 20-sec spectral level scales with M_S . The results are given in Table 3, in which all events are compared to BOXCAR (event no. 1). The results are not so good as Table 2. First of all, the M_S value of BOXCAR must have been anomalously large, by about 0.6 to 0.7 units. This could result either from release of accumulated tectonic stress by the explosion, or by development of a crack system with a preferred direction of orientation of the cracks. If the M_S value of BOXCAR is arbitrarily taken as 0.6 units less than the observed value, then the differences between ΔM_S and $\Delta \log_{10} A(20 \text{ sec})$ in Table 3 are no greater than 0.3 units for the events studied. Or, to put it in another way, if HALF BEAK is taken as the standard for comparison, then all the events except BOXCAR in Table 3 show a difference between ΔM_S and $\Delta \log_{10} A(20 \text{ sec})$ of 0.3 units or less. As the phenomenon of anomalously large surface-wave generation by release of tectonic stress or by extensive cracking is to be expected only for very large events (of the size of BOXCAR), we can conclude for the somewhat smaller events, of more interest from a detection and discrimination standpoint, that the 20-sec period spectral level of the P-wave ground motion will scale as M_S .

P-Wave Ground-Motion Spectra From MILROW (Aleutian Islands) and USSR Explosions

Spectra of the P-wave ground motion were determined from single-station observations for 6 USSR explosions and for MILROW, which took place in the Aleutian Islands. For one USSR explosion in Novaya Zemlya the spectrum was determined also from a long-period seismogram. In addition to the Novaya Zemlya event there were 4 in Kazakhstan and one in western Russia.

TABLE 3

DIFFERENCES IN M_S AND $\log_{10} A(20 \text{ sec})$ FOR SELECTED
NTS EVENTS, COMPARED TO BOXCAR

Number	Name	ΔM_S	$\Delta \log_{10} A(20 \text{ sec})$
1	BOXCAR	---	---
2	HALF BEAK	0.6	0.2
3	ZAZA	1.35	0.8
4	BRONZE	1.9	1.1
5	DURYEA	1.75	1.1
6	CHARTREUSE	1.8	1.1
7	CUP	1.6	1.1
8	DISCUS THROWER	2.3	1.4

Figure 4 shows the smoothed P-wave ground-motion spectra of the 7 events, normalized to an epicentral distance of 30° . The dashed parts of the spectra indicate extrapolations based on Murphy's (1977) theoretical curves, after they were modified to take account of absorption. Table 4 identifies the events, which are labeled A through G. The m_b values were determined by the International Seismological Centre, and the M_S values were determined by us from the amplitudes of 20-sec period Rayleigh waves.

From an examination of Figure 4 we can see that the spectral amplitude levels increase as the m_b values increase. A more quantitative comparison is given in Table 5, in which are listed the m_b and $\log_{10} A(1 \text{ sec})$ differences with respect to MILROW. From the table it appears that the $\log_{10} A(1 \text{ sec})$ value for MILROW is about 0.6 units too large. If it were reduced to the 1-sec amplitude of event B all the remaining events would scale to within 0.3 units. Looking at Figure 4, the higher-than-expected spectral level for MILROW at 1-sec period results from an apparently lower average T/Q value for it than for the Novaya Zemlya event B. An m_b value based on the single station BHP (Canal Zone) used to obtain the MILROW spectrum also was found to be about 0.6 unit higher than the average value of 6.5. The effect of the descending Pacific lithospheric slab under the Aleutians is to cause different apparent absorption for rays leaving in different azimuths, and thus it should produce different shaped spectra in different azimuths. If we had averaged the spectra for the P-wave motion of MILROW at a number of stations we probably would have arrived at a spectrum similar to that for the Novaya Zemlya event B.

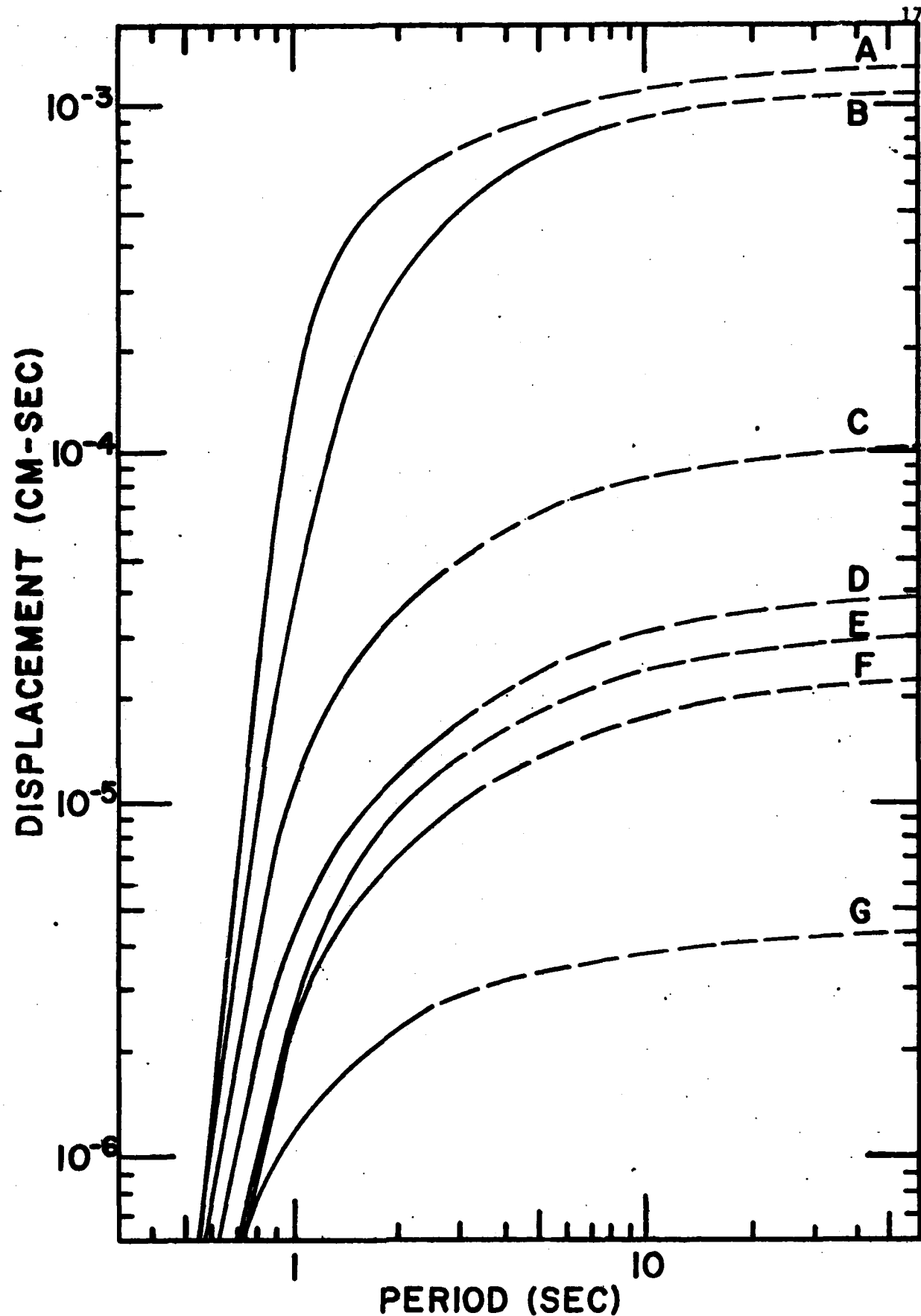


Figure 4. Smoothed P-wave ground-motion spectra normalized to 300 for MILROW and selected USSR events. The dashed-line portions of the spectra indicate extrapolations based on Murphy's (1977) modified source model. The events corresponding to the letters are identified in Table 4.

TABLE 4
SOURCE PARAMETERS OF MILROW AND SELECTED
USSR EVENTS

Letter	Location	Date	m_b	M_s
A	MILROW - Aleutians	Oct. 02, 69	6.5	5.09 ± 0.22 (40)
E	Novaya Zemlya	Sep. 27, 71	6.5	5.05 0.31 (14)
C	Kazakh	Dec. 22, 71	6.0	4.17 0.14 (8)
D	Kazakh	Oct. 21, 71	5.5	3.43 0.32 (5)
F	Kazakh	Nov. 29, 71	5.4	3.83 0.51 (5)
F	Kazakh	Oct. 09, 71	5.3	3.23 (1)
G	Western Russia	Oct. 04, 71	4.6	<2.8

TABLE 5
DIFFERENCES IN m_b AND $\log_{10} A(1 \text{ sec})$ FOR SELECTED
USSR EVENTS, COMPARED TO MILROW

Letter	Location	Δm_b	$\Delta \log_{10} A(1 \text{ sec})$
A	Aleutians (MILROW)	---	---
B	Novaya Zemlya	0.0	0.6
C	Kazakh	0.5	1.1
D	Kazakh	1.0	1.5
E	Kazakh	1.1	1.7
F	Kazakh	1.2	1.8
G	Western Russia	1.9	2.1

Table 6 shows that the differences of M_S and $\log_{10} A(20 \text{ sec})$ with respect to MILROW are all within 0.2 units except for event E, whose M_S value had a very high standard deviation (0.51). Thus probably the M_S value of event E is too large. With that single exception the M_S values scale as the 20-sec period spectral P-wave amplitudes. This indicates that none of the 7 events had anomalously large surface wave generation, as was noted for BOXCAR.

Comparison of USSR and NTS Spectra

Figure 5 compares the P-wave spectra of some NTS events (solid lines) and USSR events (dashed lines), all normalized to an epicentral distance of 30° . The figure shows that events at NTS and in Eurasia of the same M_S have similar 20-sec P-wave spectral levels, and furthermore that at the shorter periods the USSR spectra indicate somewhat lower absorption than the NTS spectra. This latter observation has two important consequences: 1) a USSR explosion of a given yield will have a higher m_b value than an NTS explosion of the same yield (the m_b difference will be about 0.3 units for an event about the size of CHARTREUSE), 2) there will be some regional dependence of the $m_b:M_S$ relation for explosions, because for a given M_S the m_b value of the explosion will depend on the P-wave absorption in the source region. In terms of T/Q, the average T/Q for NTS events is about 1.0, whereas for Kazakh events, it is about 0.8.

Summary and Conclusions

Murphy's (1977) spectra for a nuclear explosion source model were compared with P-wave ground-motion spectra at 30° epicentral distance

TABLE 6

DIFFERENCES IN M_S AND $\log_{10} A(20 \text{ sec})$ FOR
SELECTED USSR EVENTS, COMPARED TO MILROW

Letter	Location	ΔM_S	$\Delta \log_{10} A(20 \text{ sec})$
A	Aleutians (MILROW)	---	---
B	Novaya Zemlya	0.0	0.1
C	Kazakh	0.9	1.1
D	Kazakh	1.7	1.5
E	Kazakh	1.3	1.7
F	Kazakh	1.9	1.8
G	Western Russia	> 2.3	2.5

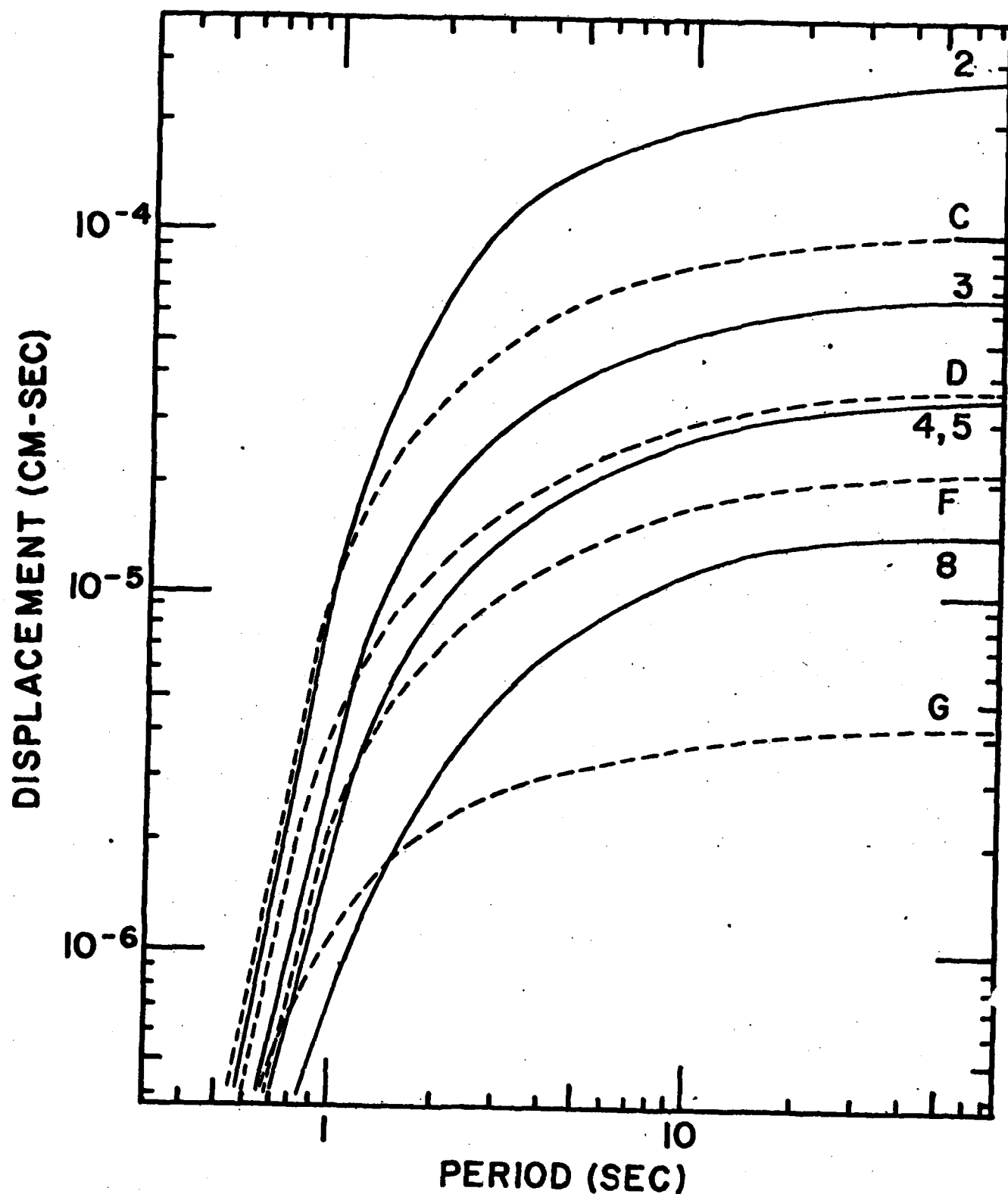


Figure 5. Smoothed P-wave ground-motion spectra normalized to 30° for selected NTS events (solid lines) and selected USSR events (dashed lines). Note that the USSR explosion spectra cross the NTS explosion spectra at the shorter periods, indicating smaller absorption in the USSR (Fazakh) test site region than at NTS.

from NTS, USSR and an Aleutian explosion. For the NTS and Kazakh test sites the $\log_{10} A(1 \text{ sec})$, where $A(1 \text{ sec})$ is the amplitude of the P-wave spectrum at 1-sec period, scaled directly as m_b . Similarly, the $\log_{10} A(20 \text{ sec})$ scaled directly as M_s , except for BOXCAR which had anomalously large surface waves.

NTS and Kazakh spectra of events with the same M_s values had the same long-period P-wave amplitude levels. However, at the shorter periods near 1 sec the Kazakh spectra had higher amplitudes than the NTS spectra, indicating lower absorption in the Kazakh source region (average T/Q of about 0.8 for Kazakh and 1.0 for NTS). The difference amounts to about 0.3 m_b units for an event the size of CHARTREUSE. Thus a Kazakh explosion of the same yield as an NTS one will have a higher m_b value, but the same M_s value. This assumes that there is no anomalously large surface wave generation due to the release of regional stress or to extensive cracking in preferred directions in the source region.

The 1-sec period amplitudes of P waves from Aleutian explosions show a dependence on azimuth, which apparently is related to the subducting Pacific plate. This is true for amplitude measurements both in the frequency and the time domain. The M_s values do not show such an azimuthal dependence, for at periods of 20 sec the effect of the plate geometry apparently is insignificant.

Finally, the $m_b:M_s$ discriminant will show some dependence on the region of the explosion, because the m_b value is affected by absorption in the source region.

Note

Dr. Robert Masse of AFTAC, after reading a draft of this report, suggested that we look at an NTS shot in granite. We selected

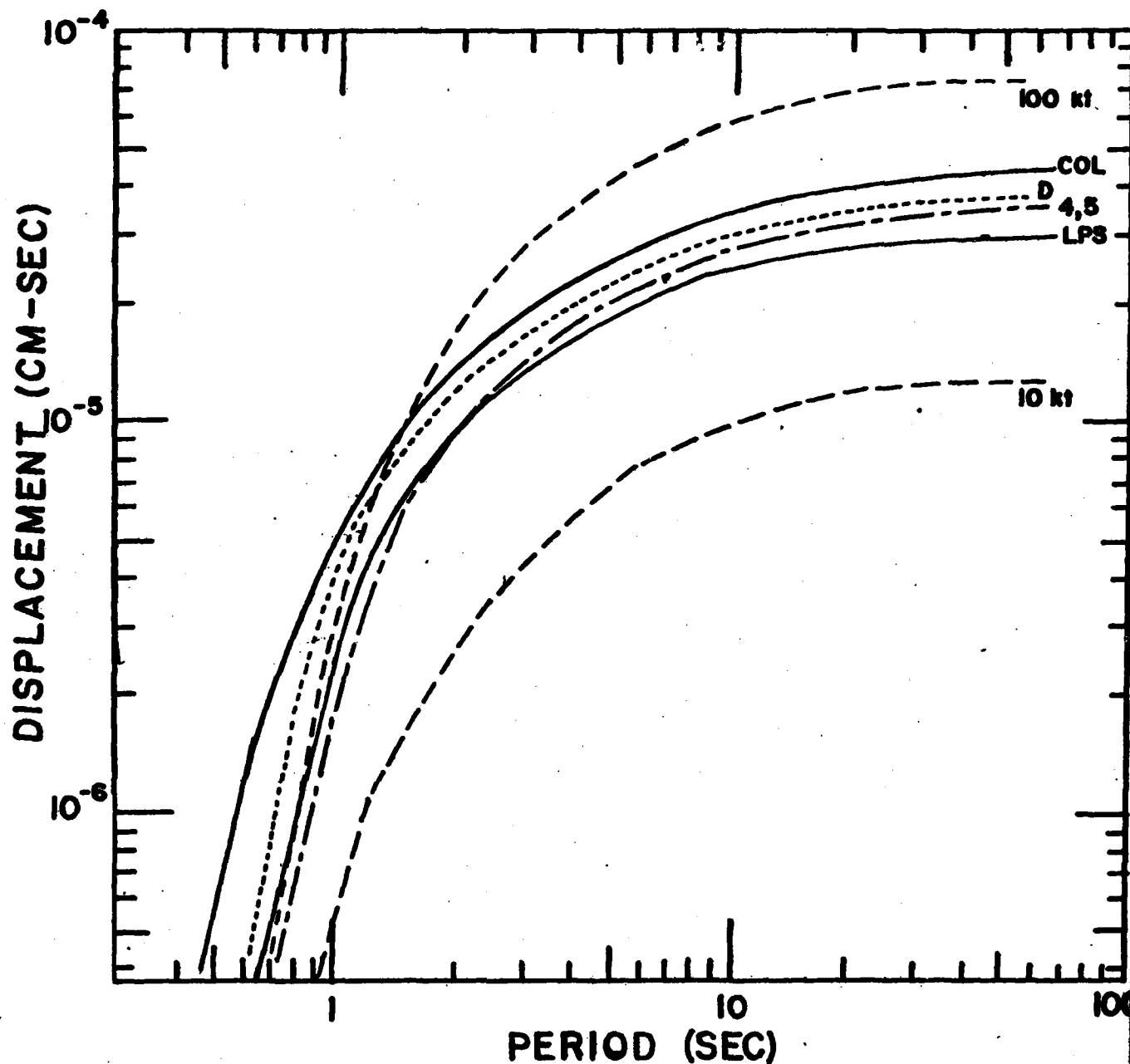


Figure 6. Smoothed P-wave spectra normalized to 300° . The solid-line curves are for the spectra of PILEDRIVER (57 kt) as recorded at COL and LPS. The long dashed-line curves are Murphy's (1977) curves for $T/Q = 1.0$ and shots of 100 kt and 10 kt yield in tuff/rhyolite. The short dashed-line curve is for Kazakh event D (see Table 4). The dash-dot curve is for NTS events 4 and 5 in tuff/rhyolite (see Table 1). Note that the PILEDRIVER curves indicate less apparent absorption, compared to the tuff/rhyolite curves, at the shorter periods. The differences in the spectral levels of the PILEDRIVER ground motion at COL and LPS suggest that absorption in the crust and upper mantle near the receiver can also affect the spectral levels.

References

- Carpenter, E. W. (1967) Teleseismic signals calculated for underground, underwater, and atmospheric explosions, Geophysics, 32, 17-32.
- Futterman, W. I. (1962) Dispersive body waves, J. Geophys. Res., 67, 5279-5291.
- Helmberger, D. V. (1973) On the structure of the low-velocity zone, Geophys. J. Roy. Ast. Soc., 34, 251-263.
- Langston, C. A., and D. V. Helmberger (1975) A procedure for modelling shallow dislocation sources, Geophys. J. Roy. Ast. Soc., 42, 117-130.
- Murphy, J. R. (1977) Seismic source functions and magnitude determinations for underground nuclear detonations, Bull. Seism. Soc. Am., 67, 135-158.
- Springer, D. L., and R. L. Kinnaman (1971) Seismic source summary for U.S. nuclear explosions, Bull. Seism. Soc. Am., 61, 1073-1098.

LOVE WAVES AS AN EXPLOSION-EARTHQUAKE DISCRIMINANT

by

Huei-Yuin Wen

Introduction

The difference in the surface-wave versus body-wave magnitude relationship between earthquakes and underground explosions was first investigated by Press et al (1963) and Brune et al (1963). Now seismologists generally agree that earthquakes and explosions can be discriminated above a certain magnitude level by using the $m_b:M_S$ criterion. For most studies (Liebermann & Pomeroy, 1969; Evernden, 1969; Basham et al, 1970; Marshall, 1970), the body-wave magnitude m_b was determined from P waves of period about 1 sec and the surface-wave magnitude M_S from the vertical-component of Rayleigh waves of period about 20 sec. Evernden (1975) found that the $M_S(20)$ for explosions was 1.0 to 1.25 units lower than that for shallow-focus earthquakes of the same m_b ($m_b > 4$). Some anomalous earthquakes (earthquakes which have $m_b:M_S$ values nearly those of explosions) occur near continental margins (Evernden, 1975) but most occur in the interior of the continent (Lander, 1972; Nuttli and Kim, 1975). For such events, the $m_b:M_S$ criterion of discrimination appears to fail.

Fundamental-mode Love waves have no node in the displacement versus depth curve. The amplitude of Rayleigh waves can have a minimum at 20-sec period for some earthquakes because of the particular depth and source mechanism, resulting in anomalously low M_S . In that case the Love-wave magnitude can be used to reclassify these earthquakes as non-anomalous

ones. Evernden (1975) found that for underground explosions the Love-wave amplitudes are significantly less than the Rayleigh-wave amplitudes, whereas for earthquakes they are of about the same value. Therefore, a $m_b:M_S$ criterion based on Love waves (M_S^L) should be more powerful than one based on Rayleigh waves (M_S^R). In addition, use of both $m_b:M_S^{RZ}$ and $M_S^L:M_S^{RZ}$ criteria should greatly improve identification capabilities.

A recent study (Nuttli et al., 1975) has shown that some aftershocks or foreshocks of non-anomalous mainshocks in the continental interior of Eurasia possessed anomalous $m_b:M_S^{RZ}$ values. In this paper, nine Eurasian events with anomalously low Rayleigh-wave magnitudes (from Nuttli et al., 1975) and fourteen northwestern Kashmir mainshock-aftershock sequence earthquakes which occurred during the year 1972, have been studied to testify to the usefulness of Love waves as a further discriminant between earthquakes and underground explosions. The data are obtained from 70-mm film copies of the VLPE stations and a selected number of WWSSN stations.

Love-Wave Magnitudes (M_S^L)

In order to determine M_S^L , one first must separate the Love waves from the Rayleigh-wave motion on the horizontal-component seismograms. The procedure for doing this is as follows.

First, identify the maximum amplitude wave motion with period about 20 ± 3 seconds as recorded on the long-period, horizontal-component seismograms (N-S and E-W components). Second, digitize two minutes or more of the maximum wave motion. The sampling interval and the digitization times must be the same for both N-S and E-W components. Third, resolve the digitized data into transverse component UT (due to Love-wave motion) and radial component UR (due to Rayleigh-wave motion).

After traces of the Love-wave motion are obtained, M_S^L can be calculated by the use of the IASPEI (INTERNATIONAL ASSOCIATION OF SEISMOLOGY AND PHYSICS OF THE EARTH'S INTERIOR) formula (Båth, 1969),

$$M_S^L = 3.30 + 1.66 \log_{10} \Delta + \log_{10} \frac{A}{T} \quad (25^\circ \leq \Delta \leq 140^\circ) \quad (1)$$

and the Nuttli-Kim (1975) formula,

$$M_S^L = 4.16 + 1.07 \log_{10} \Delta + \log_{10} \frac{A}{T} \quad (10^\circ \leq \Delta \leq 25^\circ) \quad (2)$$

where A (in microns) is one-half the maximum peak-to-peak amplitude of the Love waves, T is the corresponding period of 20 ± 3 seconds and Δ (in degrees) is the epicentral distance.

The M_S^L values for the nine anomalous earthquakes are given in Table 1. These anomalous Eurasian events, which occurred in the first half year of 1972, are not restricted to any single geographic area. Table 1 indicates that they took place in the area of $10^\circ - 50^\circ N$ and $14^\circ - 95^\circ E$. Events No. 45 and 145 are oceanic earthquakes, whereas the others are continental events. The focal depths determined by NEIC were all shallow. The probable factors influencing the $m_b : M_S^{RZ}$ relationship have been attributed to focal depth, focal mechanism, uncertainties in the crustal thickness, travel path, source-time function and the finiteness of the source (Tsai and Aki, 1971; Liebermann and Pomeroy, 1970; Evernden, 1975).

For a normal earthquake, Love waves are at least as high in amplitude as Rayleigh waves, if not larger, if an adequate number of azimuths is sampled. Evernden (1969) found that some anomalous earthquakes occurred

in Eurasia having larger Love than Rayleigh waves. By the $M_S^{RZ}:M_S^L$ criterion, the number of anomalous earthquakes is reduced to six (events which lie above either the long or short dashed lines in Figure 1).

The northwestern Kashmir mainshock-aftershock sequence consisted of 14 earthquakes with m_b values in the range of 4 to 6 that occurred during one month of 1972 and which had small variations in hypocentral coordinates and focal depths (estimated by NEIC). An advantage of using aftershocks is that it removes the propagation effect, if the earthquakes are compared to one another and if the data of the same stations are used for all the earthquakes.

Table 2 gives magnitudes and hypocentral coordinates of the Kashmir earthquakes. All earthquakes of the sequence except for the mainshock had $0.59 < m_b - M_S^{RZ} < 1.26$. In general if the difference exceeds unity the earthquakes are in or near the explosion population. These observed differences between m_b and M_S^{RZ} therefore indicate that some of the aftershocks have explosion-like $m_b:M_S^{RZ}$ values.

Figures 2 and 3 are the plots of $m_b:M_S^{RZ}$ and $m_b:M_S^L$ values for all the earthquakes. On the $m_b:M_S^{RZ}$ discriminant (Figure 2), the mainshock which occurred on September 3, 1972, of $m_b = 5.97$ and $M_S^{RZ} = 6.05$, appears to fall on the earthquake side of the curve, whereas the majority of aftershocks appear on the fringe of the earthquake $m_b:M_S^{RZ}$ population. The anomalous $m_b:M_S^{RZ}$ events, namely K3, K4, K7, and K12, switch to the earthquake part in the $m_b:M_S^L$ plots, as seen in Figure 3. All the events have Love waves at least as large in magnitude as the Rayleigh waves. Except in a region displaying very high tectonic stress release, the ratio of Love-wave to Rayleigh-wave magnitude of earthquakes is not the same as explosions, even multi-shot ones (Evernden, 1976). Therefore, when both $m_b:M_S^{RZ}$ and $m_b:M_S^L$

criteria are employed, there is compensation for any effects of the Rayleigh-wave radiation pattern, and we can conclude that the 14 Kashmir earthquakes are all non-anomalous earthquakes.

Focal Mechanisms of Kashmir Earthquakes

The fault-plane solutions for the events of the Kashmir mainshock-aftershock sequence are given in Figure 4. The P-wave polarities were determined from the long-period, vertical-component seismograms. For some stations, the first arrival of the P-wave on the short-period, vertical-component seismograms was used when the long-period, first P-wave motion was not available. The octagons and triangles stand for compressional and dilatational P-wave motion, respectively.

The focal mechanism solutions for events K1 and K7 (Figures 4(a) and 4(g)) are well determined and are similar to each other. They both are characteristic of thrust faulting, with nodal planes striking nearly in the north direction. For the remaining events a unique fault-plane solution could not be obtained from the P-wave data alone. But for these remaining earthquakes the available data are compatible with the same focal mechanism for most of the Kashmir earthquakes. The exceptions are event K8, which shows normal faulting, and event K11 which has only two readings of P-wave polarities from available seismic stations.

Love-Wave Amplitude Spectra (A_S^L)

Because all the events are intermediate to small magnitude events and because some of the records had microseisms too high to detect the surface waves, both the Love-wave magnitudes and the Love-wave amplitude

amplitude spectra have been determined with great effort and with difficulty.

The spectral amplitude of fundamental-mode Love waves in the period range 10 to 50 seconds were computed by digitizing, rotating coordinates and Fourier analyzing the resultant transverse-component digital data. The spectra were corrected for instrument response and for linear trend. They were then normalized to a reference distance of 9.0° (1000 km) from the epicenter by removing the effects of geometrical spreading, using a filter program (Herrmann, 1973). Figures 5 and 6 give sample spectra for Eurasian events whose records could be digitized, to see how they scale over the period range considered. The spectral shape should also be compared for individual events.

Tsai and Aki (1971) pointed out that the differences in amplitude spectral shape of Love waves between explosions and small earthquakes do not significantly depend on the source mechanism and focal depth, nor crustal thickness. This implies that the differences in the spectral shape of Love waves might be due to multi-pathing, lateral variation in velocity, attenuation and radiation pattern. By inspection of Figures 5 and 6, some systematic patterns emerge.

From a single station (KON) observation for event No. 37, the spectral shape resembles that of a normal shallow earthquake (Figures 6 and 7 of Tsai and Aki, 1971); the Love-wave spectrum peaks at a period of about 20 sec and decreases at the longer periods. Figure 5(b) shows Love-wave spectral shapes somewhat unlike that given for event No. 37. The spectral level increases from 20 to 40 sec, indicating a somewhat deeper focus. Over the period range of 10 to 20 sec, the spectra have relatively steep

short-period decay rates, because the short-period waves are absorbed by the water layer.

Concerning the remaining events, the data indicate that events No. 73, 145, and 146 all generate Love waves with spectral content similar to event No. 45, whereas event No. 135 and almost all the Kashmir earthquakes (Figures 5(d) and 6) have shallow focus characteristics. If the focal depths of those events as determined by NEIC are correct, it is inferred that differences in the prevailing periods of surface waves, as indicated by the ratio of the amplitude spectral density of 20/40-sec Love waves, will indicate whether these shallow earthquakes are anomalous or non-anomalous if the ratio is less than or greater than one, respectively. Table 3 gives the relations between magnitudes and amplitude spectra (in units of cm-sec) of Love waves. If the ratio of $A_S^L(20)/A_S^L(40)$ is assumed to be independent of magnitude and source region, it can provide a discrimination capability. That is, for shallow non-anomalous earthquakes the ratio $A_S^L(20)/A_S^L(40)$ should be larger than one. By knowing that the focal depth and source mechanism of the events in the Kashmir aftershock sequence are not different, and because the propagation paths are essentially the same, the question as to how the discrepancy in the spectral shape of Love waves recorded at station SHI arises is not yet answered.

$M_S^L:A_S^L$ Relationship

From the concept of surface-wave magnitude (M_S^L) and the amplitude spectrum (A_S^L), M_S^L should have a linear relation with $\log_{10} A_S^L$ at a period of 20 sec. In addition, there is an equivalence of logarithmic amplitude differences in the time domain (ΔM_S^L) with those in the frequency domain ($\Delta \log_{10} A_S^L$). Taking the data for event No. 37 at KON as the reference value

for those nine Eurasian events and SHI for event K2 for Kashmir events, Table 3 shows (4th column and 7th column) that ΔM_S^L is almost consistent with $\Delta \log_{10} A_S^L(20)$.

A relation between Love-wave magnitudes (M_S^L) and amplitude spectra (A_S^L) at a period of 20 sec and an epicentral distance of 9° has been determined by a linear least-square fit to the data of Table 3. The regression line is

$$M_S^L = (0.902 \pm 0.113) \log_{10} A_S^L + (6.688 \pm 0.318) \quad (3)$$

which is shown in Figure 7, for 95% confidence.

Discussion and Conclusions

Love-wave magnitudes and amplitude spectra were investigated for Eurasian earthquakes. A spectral amplitude determination is superior to a magnitude determination of the size of an earthquake because it covers a range of periods. From the relation between m_b and M_S^L and the relation between M_S^L and A_S^L , a hypothesis is proposed that a more effective discriminant between earthquakes and underground explosions is one based on a comparison of body-wave magnitudes (m_b) and Love-wave amplitude spectra (A_S^L). By combinations of Figures 1, 3, and 7, the amplitude spectra data are plotted in Figure 8 as a function of body-wave magnitude for all the Eurasian events studied in the paper. This figure shows that only four events (events No. 45, 73, 145, 146) are classified as anomalous earthquakes. In addition, there was one event, No. 43, for which a Love-wave spectrum could not be determined, which was anomalous.

The following conclusions are noted from this study:

Discrimination between earthquakes and underground nuclear explosions in Eurasia by the $m_b:M_S$ criterion is enhanced when the amplitude of Love waves at a period near 20-sec, rather than Rayleigh waves (vertical-component), is used to determine M_S . In general, Love-wave magnitude can be used to reduce the number of anomalous events. Of nine Eurasian events with anomalous $m_b:M_S^{RZ}$ values, six are also anomalous earthquakes by the $m_b:M_S^L$ criterion. None of the 14 Kashmir mainshock-aftershock sequence earthquakes has been found to be anomalous although 4 events in the sequence have anomalously low Rayleigh-wave magnitudes.

The Love-wave amplitude spectrum (A_S^L) also appears to be a useful earthquake-explosion discriminant. By the $m_b:A_S^L$ criterion, only four of the Eurasian earthquakes studied were anomalous. For the remaining two events (events No. 37 and 43) with anomalous $m_b:M_S^L$ values, the shape of the Love-wave amplitude spectrum of event No. 37 has normal shallow earthquake characteristics. There are no available spectral data for event No. 43, because the surface-wave motion was too small.

For a Kashmir mainshock-aftershock sequence studied, the focal depths and focal mechanisms were the same for almost all events. Furthermore by both the $m_b:M_S^L$ and $m_b:A_S^L$ criteria, all the events in the sequence are non-anomalous. In summary, it is concluded that Love waves provide a powerful earthquake-explosion discriminant.

Although others have suggested that anomalous earthquakes are confined to the interior of the continent or to aftershock sequences, two oceanic events and none of the Kashmir aftershock sequence are found to be anomalous earthquakes by the Love-wave discriminant employed in this study. It is believed that most anomalous earthquakes can be reclassified

as non-anomalous by an adequate analysis of the available data.

References

- Basham, P.W., D.H. Weichert, and F.M. Anglin, An analysis of the 'Benham' aftershock sequence using Canadian recordings, J. Geophys. Res., 75, 1545-1556, 1970.
- Båth, M., Handbook on earthquake magnitude determinations, p. 131, Seismological Institute, Uppsala, Sweden, 1969.
- Brune, J.N., A. Espinosa, and J. Oliver, Relative excitation of surface waves by earthquakes and underground explosions in the California-Nevada region, J. Geophys. Res., 68, 3501-3513, 1963.
- Evernden, J.F., Identification of earthquakes and explosions by use of teleseismic data, J. Geophys. Res., 74, 3828-3856, 1969.
- Evernden, J.F., Further studies on seismic discrimination, Bull. Seism. Soc. Am., 65, 359-391, 1975.
- Evernden, J.F., Study of seismological evasion. Part I. General discussion of various evasion schemes, Bull. Seism. Soc. Am., 66, 245-280, 1976.
- Herrmann, R.B., Some aspects of band-pass filtering of surface waves, Bull. Seism. Soc. Am., 63, 663-671, 1973.
- Lander, T., Some interesting central Asian events on the $M_S:m_b$ diagrams, Geophys. J. Roy. Ast. Soc., 31, 329-339, 1972.
- Liebermann, R.C., and P.W. Pomeroy, Relative excitation of surface waves by earthquakes and underground explosions, J. Geophys. Res., 74, 1575-1590, 1969.
- Liebermann, R.C., and P.W. Pomeroy, Source dimensions of small earthquakes as determined from the size of the aftershock zone, Bull. Seism. Soc. Am., 60, 879-890, 1970.
- Marshall, P.D., Aspects of the spectral differences between earthquakes and underground explosions, Geophys. J. Roy. Ast. Soc., 20, 397-416, 1970.
- Nuttli, O.W., and S.G. Kim, Surface-wave magnitudes of Eurasian earthquakes and explosions, Bull. Seism. Soc. Am., 65, 693-709, 1975.
- Nuttli, O.W., S.G. Kim, and H.Y. Wen, Research in Seismology: Earthquake Magnitudes, Scientific Report No. 3, AFCRL-TR-75-0433, Air Force Cambridge Research Laboratories, Hanscom AFB, Massachusetts, 1975.
- Tsai, Y.B., and K. Aki, Amplitude spectra of surface waves from small earthquakes and underground nuclear explosions, J. Geophys. Res., 76, 3940-3952, 1971.

TABLE 1.
ANOMALOUS EARTHQUAKES STUDIED

Event ^a No.	Date	Origin ^b Time	Lat. ^b (°N)	Long. ^b (°E)	Depth ^d (km)	m_b ^{e,f,g,h}	M_S ^{e,f,g,h}	Location
37	09-02-72	11-22-51.7	43.2	46.0	(36)-N (58)-I	4.81±0.23 (4)	3.43±0.48 (4)	E. Caucasus
43	20-02-72	03-02-14.0	34.6	80.3	(33)-N (33)-I	4.79±0.21 (4)	3.43±0.91 (2)	Tibet
45	22-02-72	18-43-42.0	10.4	92.5	(33)-N (4)-I	5.43±0.36 (7)	4.56±0.22 (6)	Andaman Isl.
55	04-03-72	08-22-16.6	42.1	83.3	(33)-N (33)-I	4.53±0.40 (6)	3.43 (1)	N. Sinkiang
73	26-03-72	06-10-33.2	25.9	93.9	(33)-N (88)-I	4.63±0.07 (2)	2.76 (1)	E. India
135	30-05-72	06-38-16.8	38.3	69.5	(35)-N (20)-I	4.75±0.44 (5)	3.71±0.34 (2)	Tadzhikistan
145	14-06-72	00-49-54.4	40.1	51.9	(47)-N (39)-I	4.80±0.15 (4)	3.41±0.14 (3)	Caspian Sea
146	14-06-72	04-34-28.1	33.0	46.1	(33)-N (47)-I	5.25±0.18 (7)	4.38±0.30 (5)	Iran-Iraq
148	17-06-72	09-02-47.5	48.3	14.5	(33)-N (20)-I	4.08±0.36 (11)	2.99 (1)	Austria

The symbols "a-h" are given in Table 1.

TABLE 2
HYPOCENTRAL COORDINATES AND MAGNITUDES OF KASHMIR EARTHQUAKES STUDIED

Event ^a	Date	Origin ^b Time	Lat. ^b (°N)	Long. ^b (°E)	Depth (km) NEIC	m_b ^{e,f,g,h}	$M_S^{e,f,g,h}$	$M_S^{e,f,g,h}$
K1	03-09-72	16-48-28.8	35.96	73.35	33	5.97±0.37 (4)	6.05±0.42 (7)	4.84±0.27 (2)
K2	03-09-72	23-03-52.1	35.91	73.26	33	5.27±0.38 (7)	4.55±0.38 (9)	4.21±0.19 (4)
K3	04-09-72	01-23-49.5	35.80	73.31	33	4.87±0.55 (6)	3.61±0.30 (4)	4.18±0.11 (4)
K4	04-09-72	02-36-17.1	35.94	73.35	30	5.03±0.38 (4)	3.97±0.37 (4)	4.29±0.17 (4)
K5	04-09-72	03-51-20.9	35.93	73.46	35	4.98±0.38 (6)	4.37±0.25 (4)	4.45±0.28 (2)
K6	04-09-72	13-37-51.4	35.80	73.30	33	4.91±0.21 (5)	3.92±0.29 (6)	4.74±0.51 (4)
K7	04-09-72	13-42-18.1	35.92	73.41	33	5.35±0.46 (7)	4.46±0.53 (5)	3.82 (1)
K8	05-09-72	03-08-00.7	35.85	73.52	45	4.17±0.27 (4)	3.43±0.26 (5)	3.65 (1)
K9	05-09-72	04-07-27.0	35.87	73.41	33	4.45±0.51 (4)	3.32±0.16 (3)	3.99±0.11 (4)
K10	05-09-72	09-13-57.3	35.82	73.41	33	4.81±0.46 (6)	3.67±0.56 (3)	3.81±0.30 (2)
K11	07-09-72	04-24-15.0	35.96	73.56	33	4.40±0.13 (2)	3.38±0.37 (5)	

TABLE 3

LOVE-WAVE MAGNITUDES AND AMPLITUDE SPECTRAL DENSITIES
FOR THE EURASIAN EVENTS STUDIED

Event No.	Station	M_S^L	ΔM_S^L	$A_S^L(20)$	$\log_{10} A_S^L(20)$	$\Delta \log_{10} A_S^L(20)$	$A_S^L(40)$	$A_S^L(20)/A_S^L(40)$
37	KON	3.85	0	1.053×10^{-3}	-2.978	0	8.755×10^{-4}	1.203
	KBL	2.95	-0.90	4.878×10^{-5}	-4.312	-1.334	---	---
	(av.)			5.509×10^{-4}				1.203
45	CHG	4.49	0.64	7.772×10^{-3}	-2.109	0.869	1.794×10^{-2}	0.433
	CTA	---	---	6.719×10^{-4}	-3.173	-0.195	9.135×10^{-3}	0.073
	KBL	4.21	0.36	1.150×10^{-3}	-2.939	0.039	6.718×10^{-3}	0.171
	SHI	4.49	0.64	3.140×10^{-3}	-2.503	0.475	7.788×10^{-3}	0.403
	(av.)			3.183×10^{-3}				0.270
73	CHG	2.76	-1.09	7.754×10^{-5}	-4.111	-1.133	2.026×10^{-4}	0.383
135	QUE	3.95	0.10	2.091×10^{-3}	-2.680	0.298	1.388×10^{-3}	1.506
145	KBL	3.52	-0.33	2.995×10^{-4}	-3.524	-0.546	3.291×10^{-4}	0.910

TABLE 3 (Cont'd)

LOVE-WAVE MAGNITUDES AND AMPLITUDE SPECTRAL DENSITIES
FOR THE EURASIAN EVENTS STUDIED

Event No.	Station	M_S^L	ΔM_S^L	$A_S^L(20)$	$\log_{10} A_S^L(20)$	$\Delta \log_{10} A_S^L(20)$	$A_S^L(40)$	$A_S^L(20)/A_S^L(40)$
	QUE	3.43	-0.42	2.448×10^{-4}	-3.611	-0.633	7.296×10^{-4}	0.336
	(av.)			2.721×10^{-4}				0.623
146	AAE	4.30	0.45	3.308×10^{-3}	-2.480	0.498	2.571×10^{-3}	1.286
	AQU	4.23	0.38	1.582×10^{-3}	-2.801	0.177	2.995×10^{-3}	0.528
	NIL	4.82	0.97	6.162×10^{-3}	-2.210	0.768	5.178×10^{-3}	1.190
	QUR	4.52	0.67	3.993×10^{-3}	-2.399	0.579	4.480×10^{-3}	0.891
	TRI	4.02	0.17	1.261×10^{-3}	-2.899	0.079	1.923×10^{-3}	0.655
	(av.)			3.261×10^{-3}				0.910
148	TLO	---	---	1.730×10^{-4}	-3.762	0.784	---	---

* The spectra were all normalized to an epicentral distance of 9° .

TABLE 3 (Con't)

LOVE-WAVE MAGNITUDES AND AMPLITUDE SPECTRAL* DENSITIES
FOR THE EURASIAN EVENTS STUDIED

Event	Station	M_S^L	ΔM_S^L	$A_S^L(20)$	$\log_{10} A_S^L(20)$	$\Delta \log_{10} A_S^L(20)$	$A_S^L(40)$	$A_S^L(20)/A_S^L(40)$
K2	SHI	5.03	0	1.281×10^{-2}	-1.893	0	1.185×10^{-2}	1.08
K3	EIL	3.95	-1.08	8.446×10^{-4}	-3.073	-1.180	6.250×10^{-4}	1.351
	KON	4.33	-0.70	1.062×10^{-3}	-2.974	-1.081	7.446×10^{-4}	1.426
	QUE	4.18	-0.85	2.109×10^{-3}	-2.676	-0.783	9.662×10^{-4}	2.192
	SHI	4.37	-0.66	2.260×10^{-3}	-2.646	-0.753	2.896×10^{-3}	0.780
	(av.)			1.569×10^{-3}				1.437
K4	EIL	4.09	-0.94	8.000×10^{-4}	-3.097	-1.204	7.875×10^{-4}	1.016
	QUE	4.09	-0.94	3.011×10^{-3}	-2.521	-0.628	---	---
	SHI	4.31	-0.72	2.664×10^{-3}	-2.574	-0.681	2.473×10^{-3}	1.077
	(av.)			2.158×10^{-3}				1.047
K5	EIL	4.25	-0.78	1.831×10^{-3}	-2.737	-0.844	1.002×10^{-3}	1.826

TABLE 3 (Cont'd)

LOVE-WAVE MAGNITUDES AND AMPLITUDE SPECTRAL DENSITIES
FOR THE EURASIAN EVENTS STUDIED

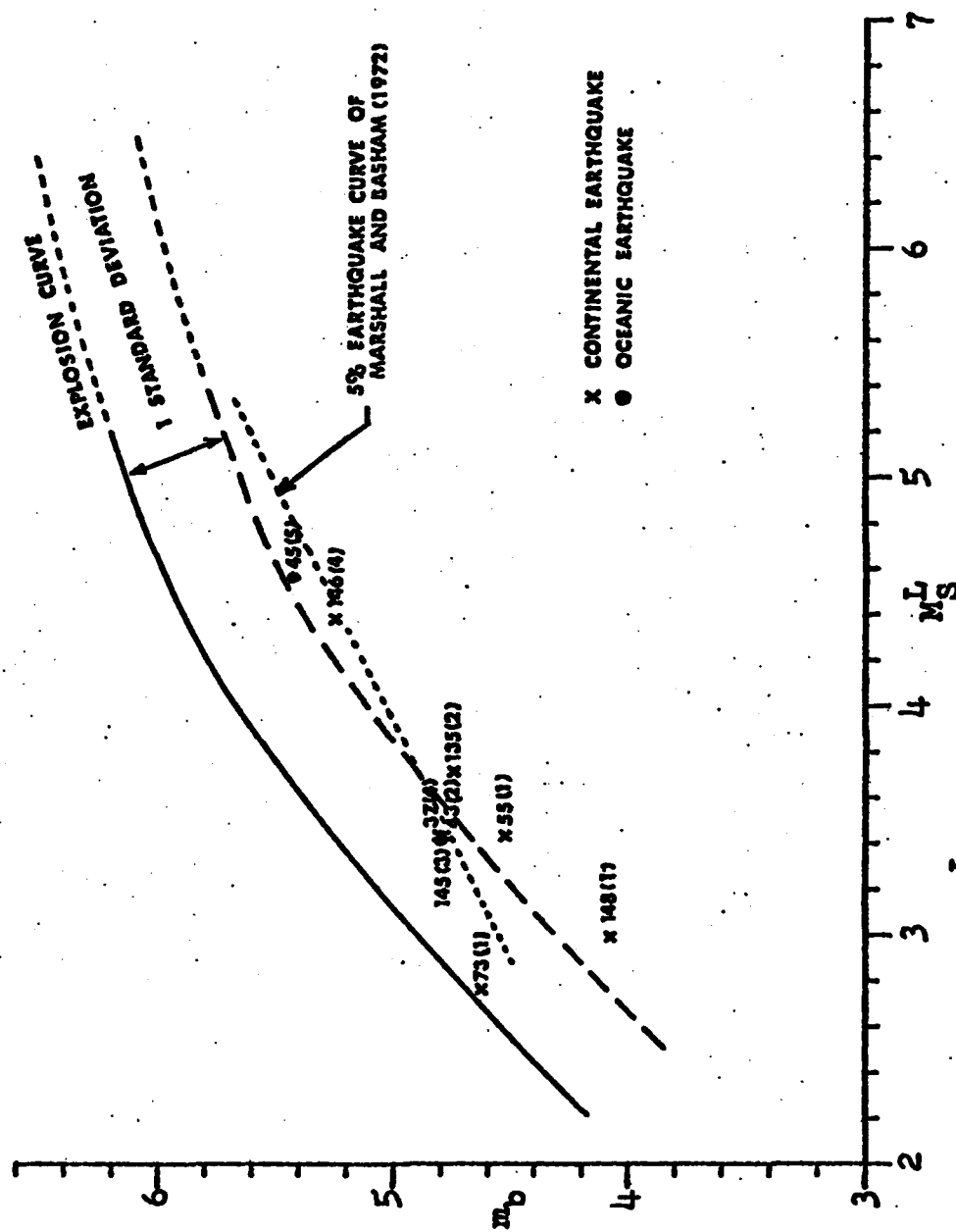
Event Station	M_S^L	ΔM_S^L	$A_S^L(20)$	$\log_{10} A_S^L(20)$	$\Delta \log_{10} A_S^L(20)$	$A_S^L(40)$	$A_S^L(20)/A_S^L(40)$
QUE	4.34	-0.69	4.22×10^{-3}	-2.374	-0.481	---	---
SHI	4.49	-0.54	3.85×10^{-3}	-2.414	-0.521	3.012×10^{-3}	1.278
(av.)			3.302×10^{-3}				1.552
K6 SHI	4.25	-0.78	1.874×10^{-3}	-2.727	-0.834	1.261×10^{-3}	1.486
K7 CHG	4.05	-0.98	9.467×10^{-3}	-3.024	-1.121	---	---
EIL	4.65	-0.38	5.050×10^{-3}	-2.297	-0.404	2.582×10^{-3}	1.956
KON	5.08	0.05	4.857×10^{-3}	-2.314	-0.421	3.716×10^{-3}	1.307
SHI	5.17	0.14	1.607×10^{-2}	-1.794	0.099	1.694×10^{-2}	0.948
(av.)			6.731×10^{-3}				1.404
K10 EIL	3.87	-1.16	6.934×10^{-4}	-3.159	-1.266	2.996×10^{-4}	2.014
SHI	3.93	-1.10	9.556×10^{-4}	-3.020	-1.127	---	---

TABLE 3 (Cont'd)

LOVE-WAVE MAGNITUDES AND AMPLITUDE SPECTRAL* DENSITIES
FOR THE EURASIAN EVENTS STUDIED

Event Station	M_S^L	ΔM_S^L	$A_S^L(20)$	$\log_{10} A_S^L(20)$	$\Delta \log_{10} A_S^L(20)$	$A_S^L(40)$	$A_S^L(20)/A_S^L(40)$
QUE	4.10	-0.93	9.158×10^{-4}	-3.038	-1.135	---	---
(av.)			8.548×10^{-4}				2.014
K11 QUE	3.59	-1.44	1.052×10^{-3}	-2.978	-1.085	---	---
SHI	4.02	-1.01	1.348×10^{-3}	-2.870	-0.977	1.057×10^{-3}	1.276
(av.)			1.200×10^{-3}				1.276
K12 CHG	---	---	1.335×10^{-3}	-2.874	-0.981	---	---
EIL	4.51	-0.52	2.150×10^{-3}	-2.688	-0.795	1.586×10^{-3}	1.356
SHI	4.99	-0.04	1.201×10^{-2}	-1.921	-0.028	1.257×10^{-2}	0.955
(av.)			5.165×10^{-3}				1.156
K14 SHI	4.25	-0.78	2.324×10^{-3}	-2.634	-0.741	3.090×10^{-3}	0.752

* The spectra were all normalized to an epicentral distance of 9° .



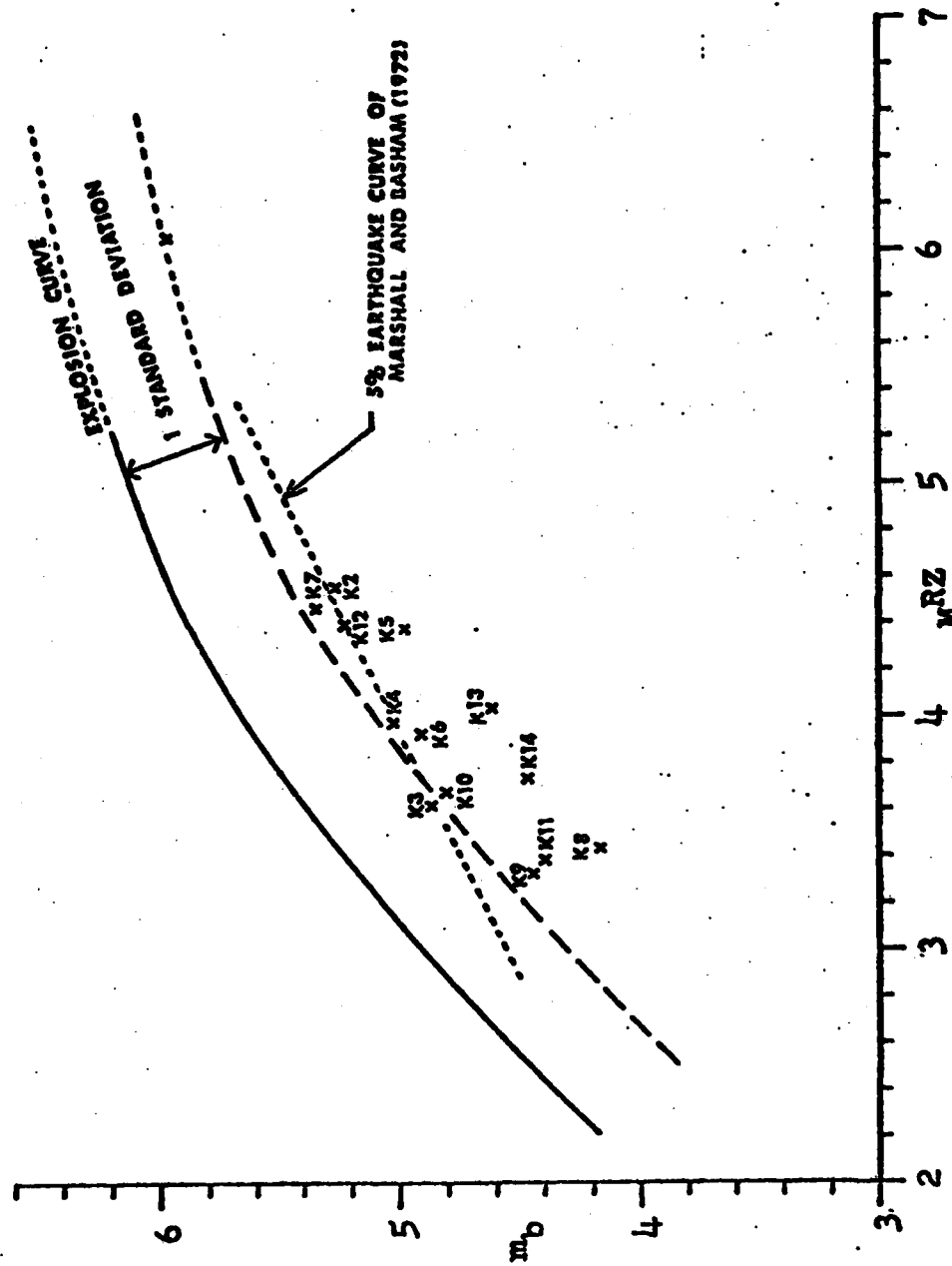


Figure 2. m_b versus M_S values for northwestern Kashmir mainshock-aftershock sequence.

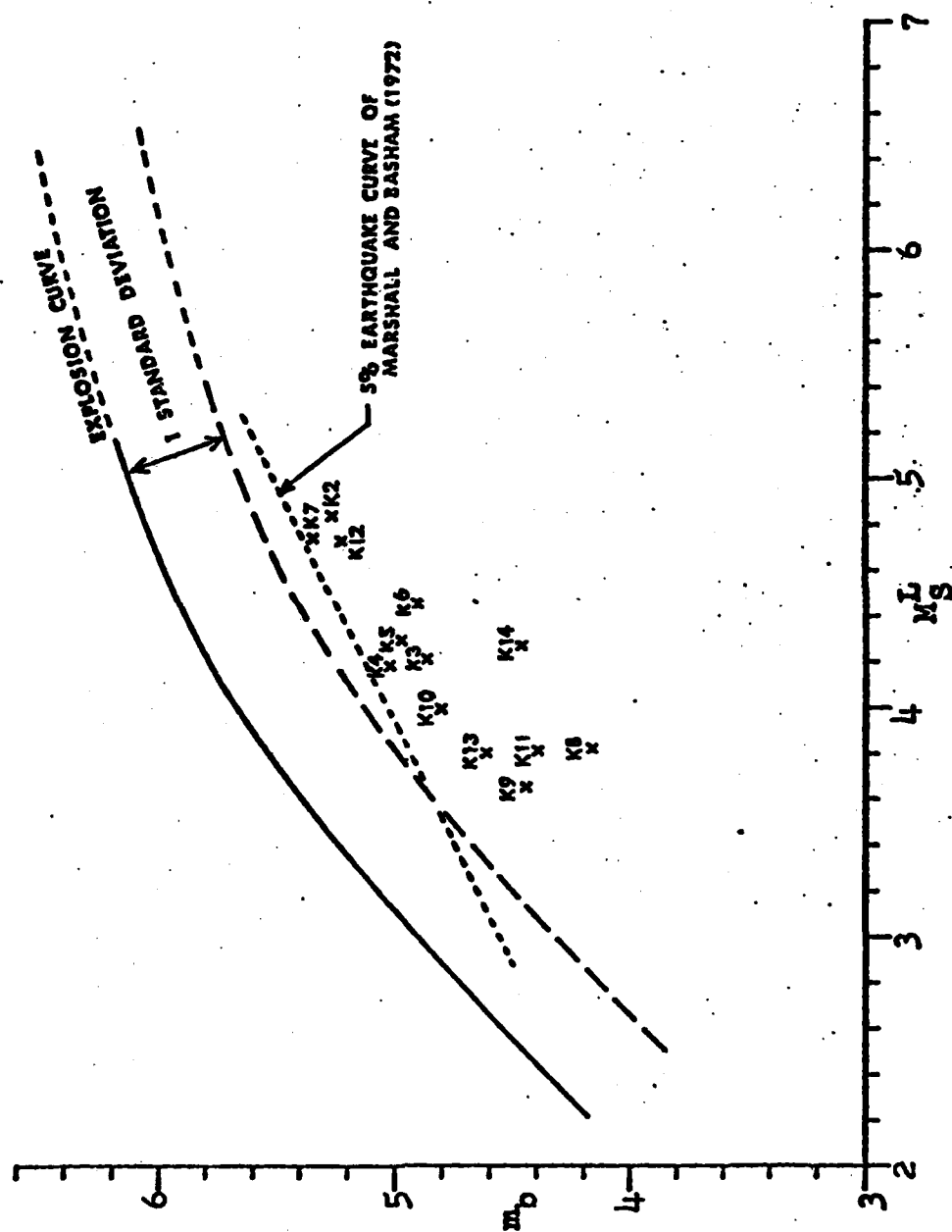


Figure 3. m_b versus M_S^L values for northwestern Kashmir mainshock-aftershock sequence.

EVENT K1

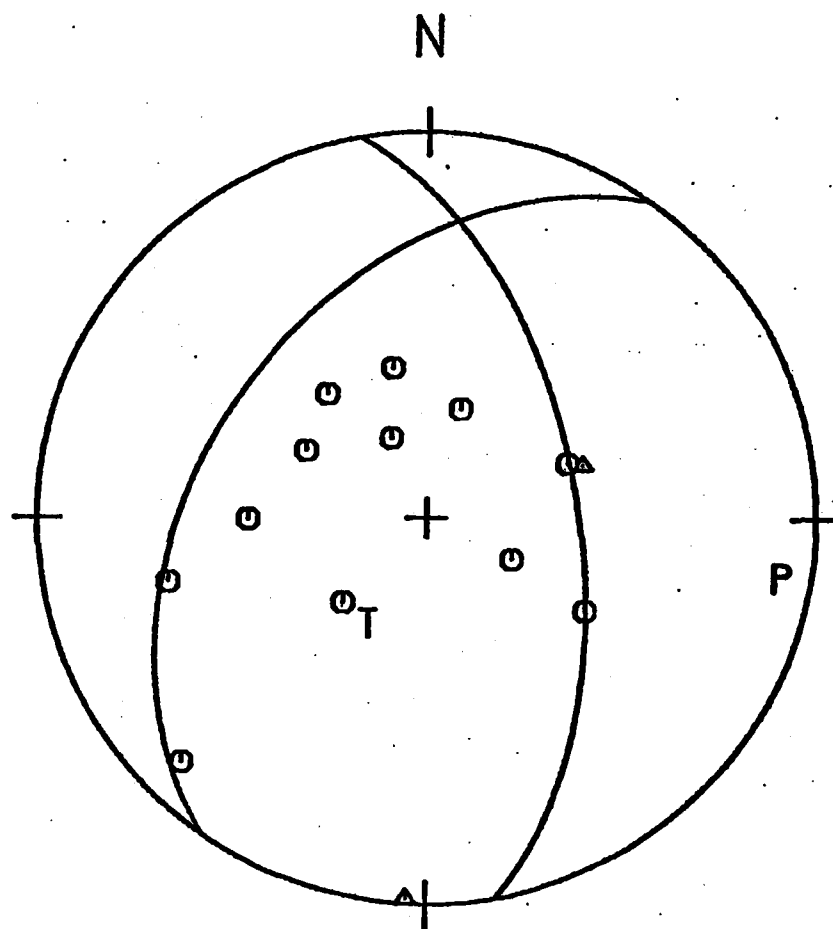


Figure 4a. Fault-plane solution for event K1 of the northwestern Kashmir mainshock-aftershock sequence. The octagons and triangles stand for compressional and dilatational P-wave motion, respectively.

EVENT K2

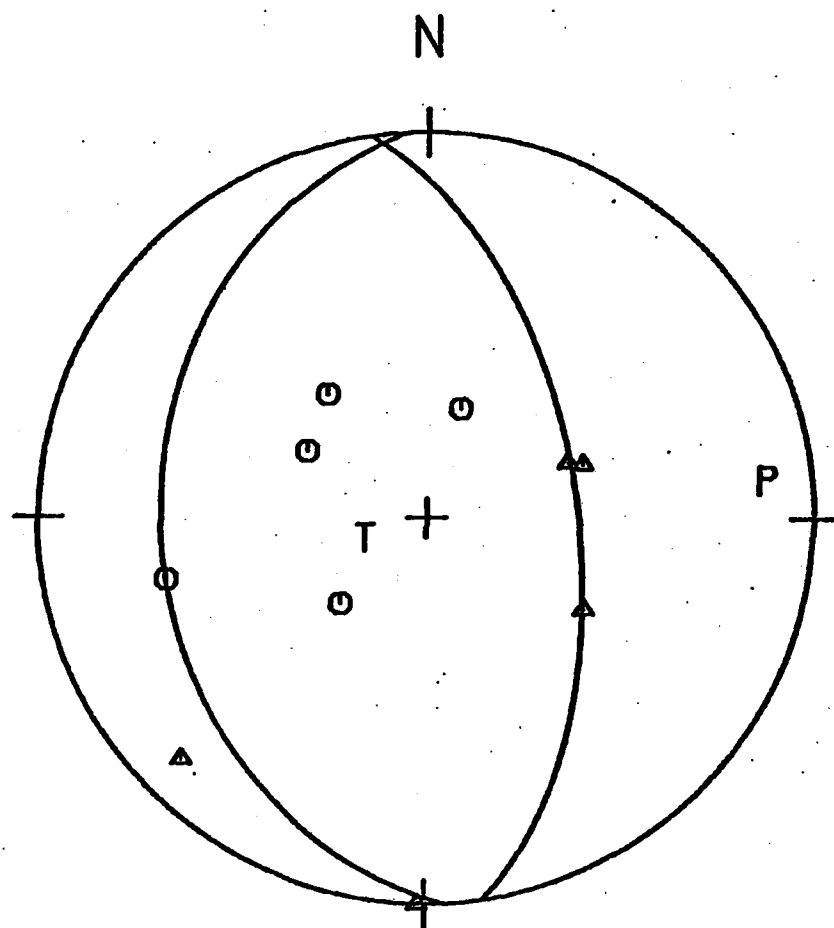


Figure 4b. Fault-plane solution for event K2 of the northwestern Kashmir mainshock-aftershock sequence.

EVENT K3

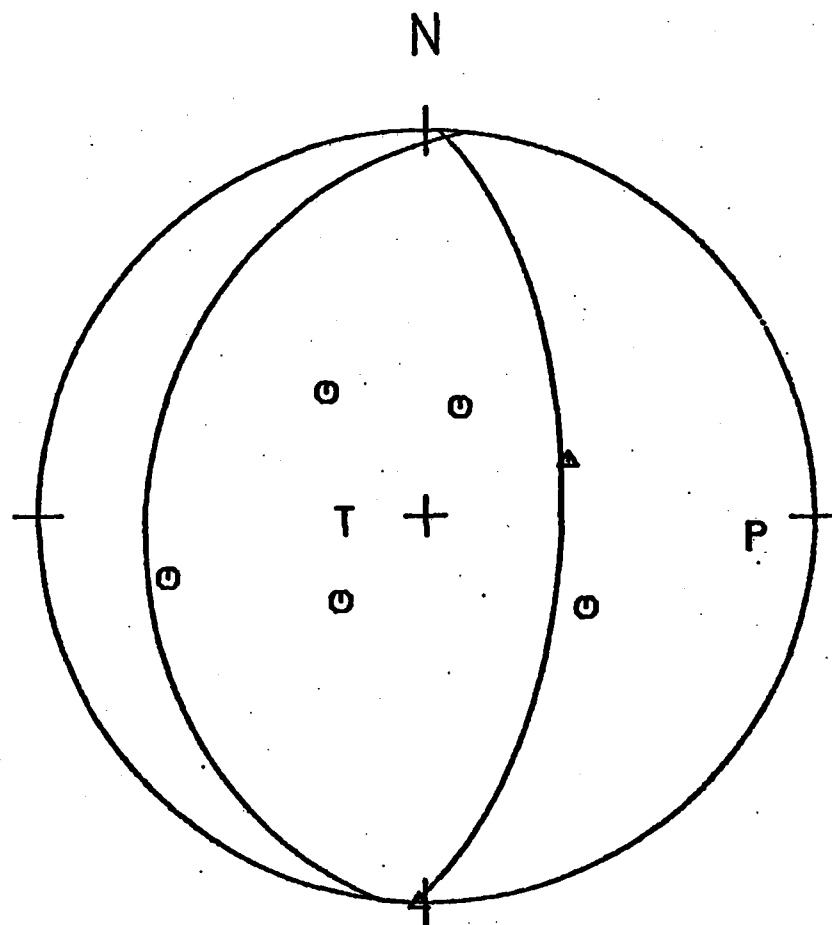


Figure 4c. Fault-plane solution for event K3 of the northwestern Kashmir mainshock-aftershock sequence.

EVENT K4

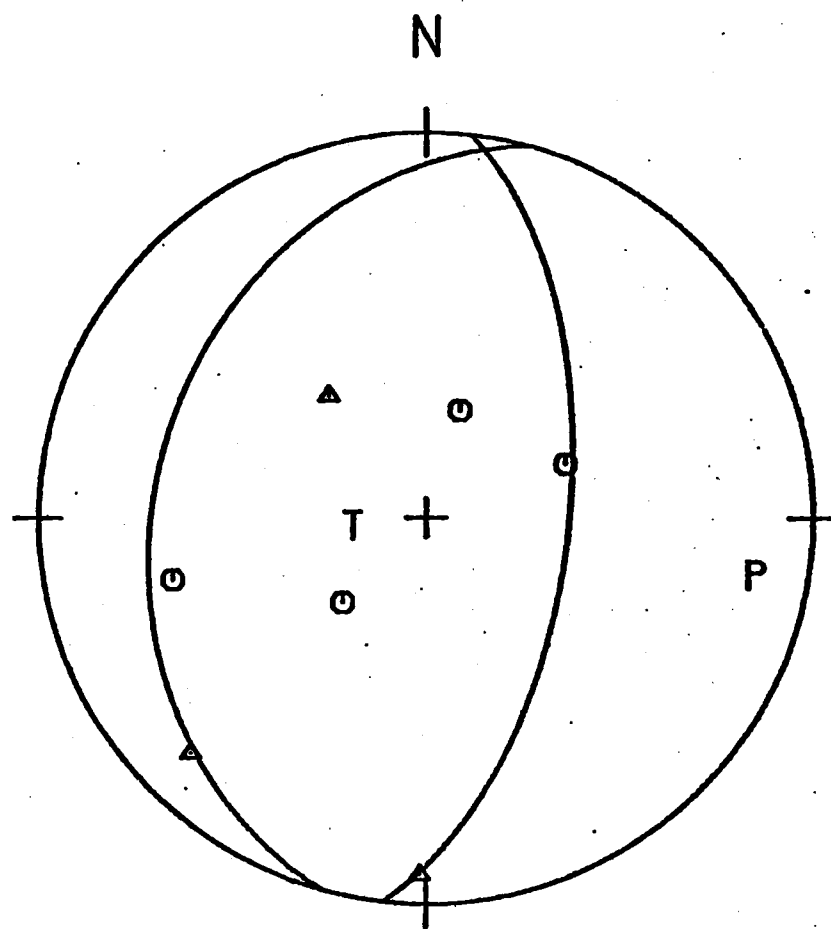


Figure 4d . Fault-plane solution for event K4 of the northwestern Kashmir mainshock-aftershock sequence.

EVENT K5

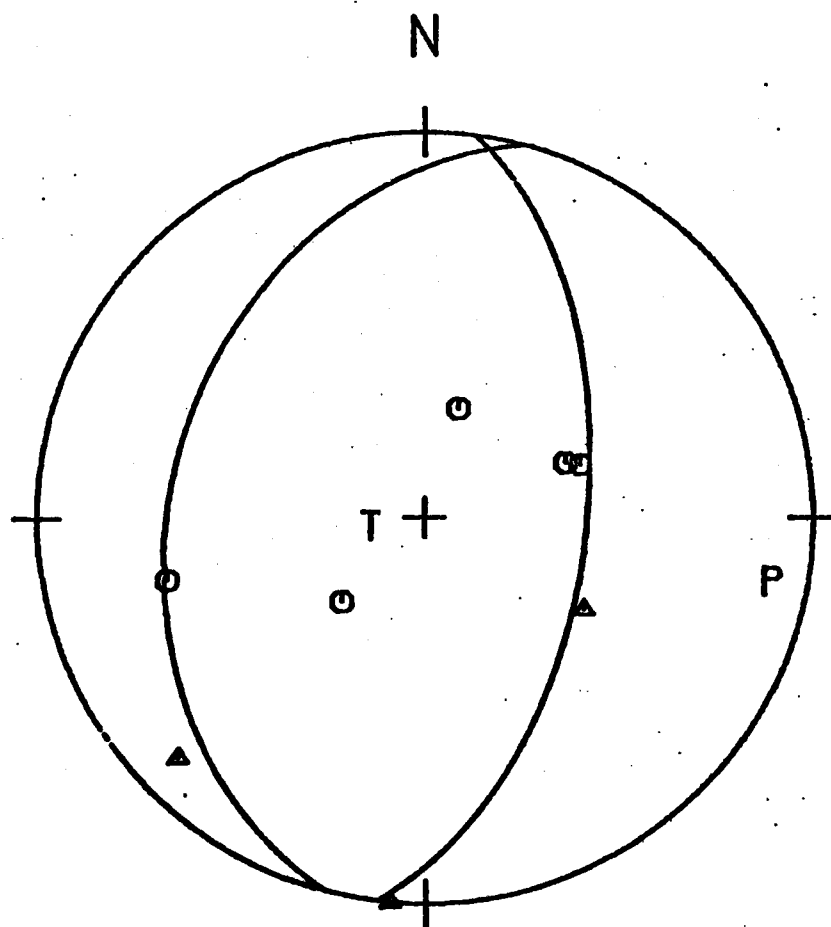


Figure 4c. Fault-plane solution for event K5 of the northwestern Kashmir mainshock-aftershock sequence.

EVENT K6

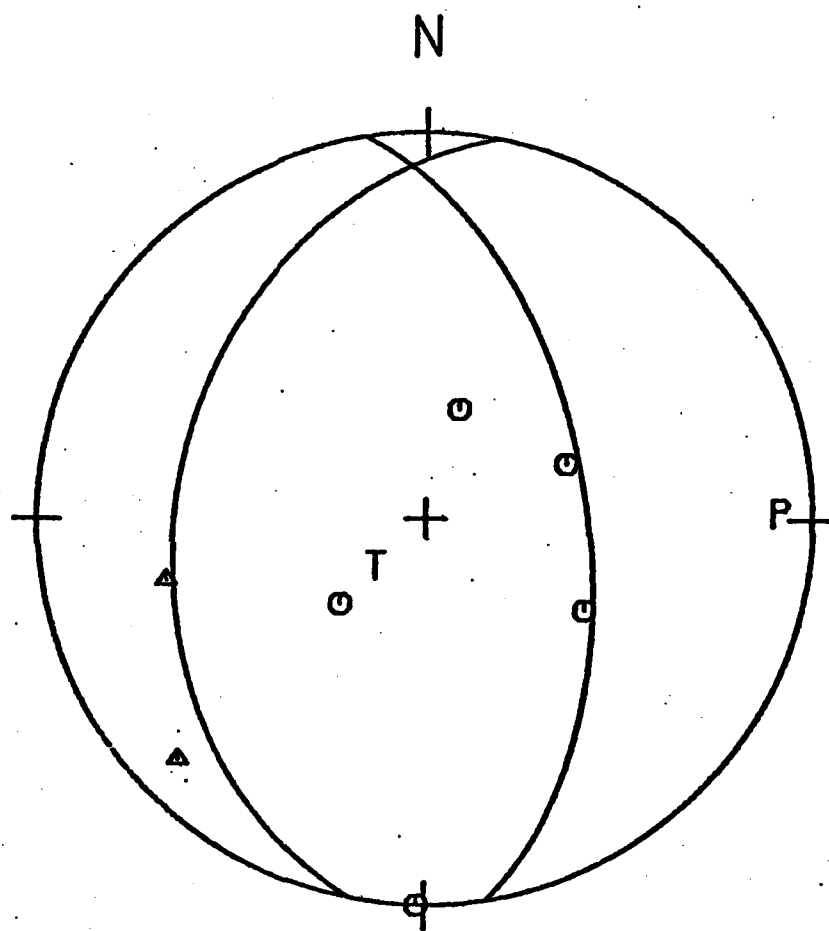


Figure 4f. Fault-plane solution for event K6 of the northwestern Kashmir mainshock-aftershock sequence.

EVENT K7

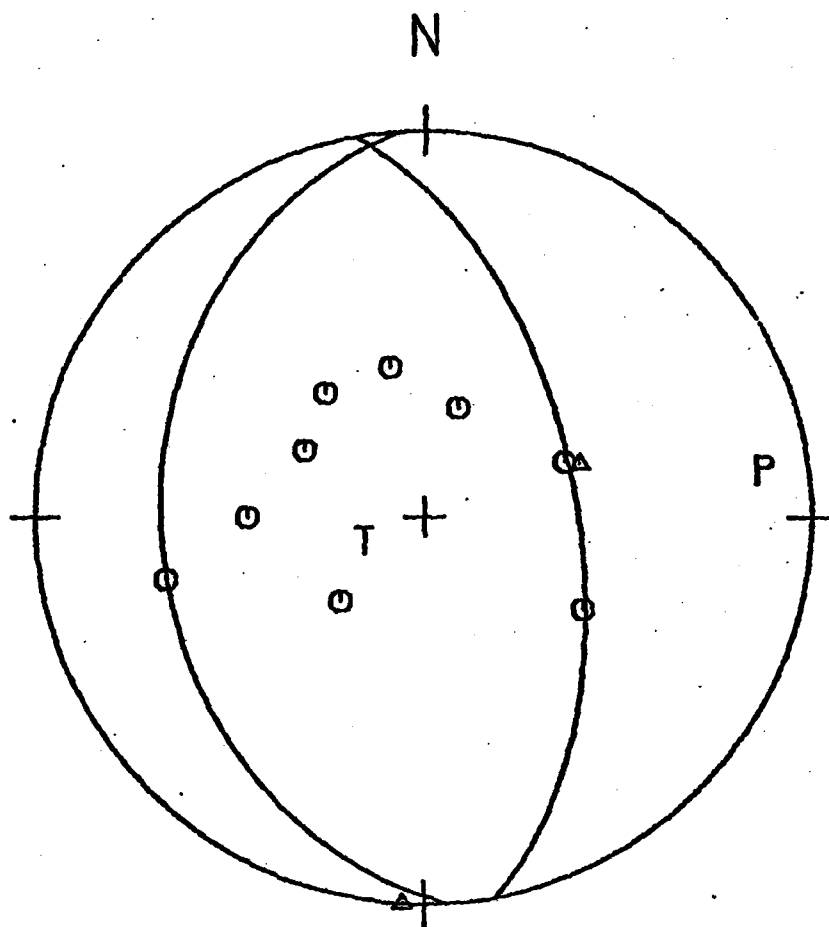


Figure 4g. Fault-plane solution for event K7 of the northwestern Kashmir mainshock-aftershock sequence.

EVENT K8

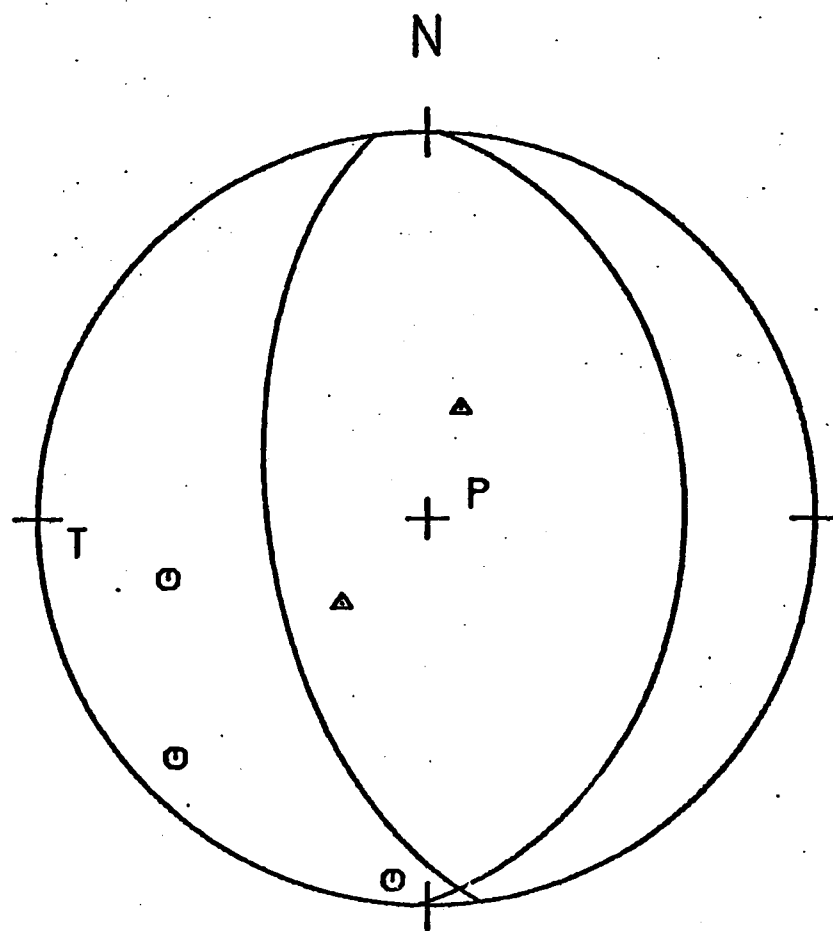


Figure 4h. Fault-plane solution for event K8 of the northwestern Kashmir mainshock-aftershock sequence.

EVENT K9

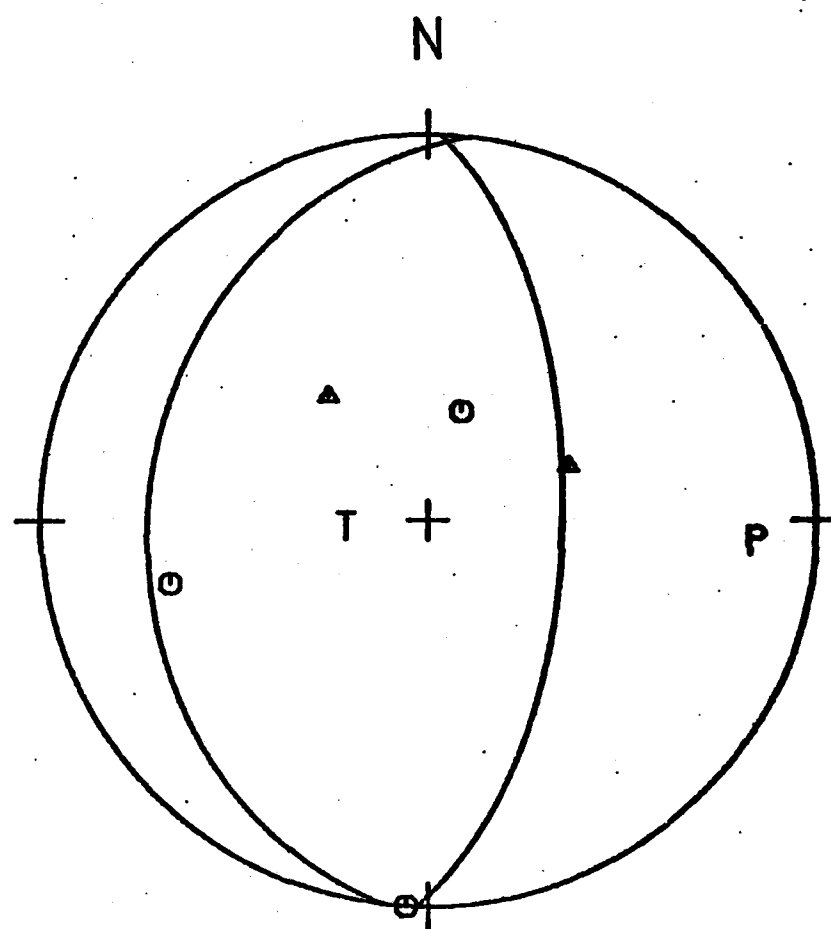


Figure 4i. Fault-plane solution for event K9 of the northwestern Kashmir mainshock-aftershock sequence.

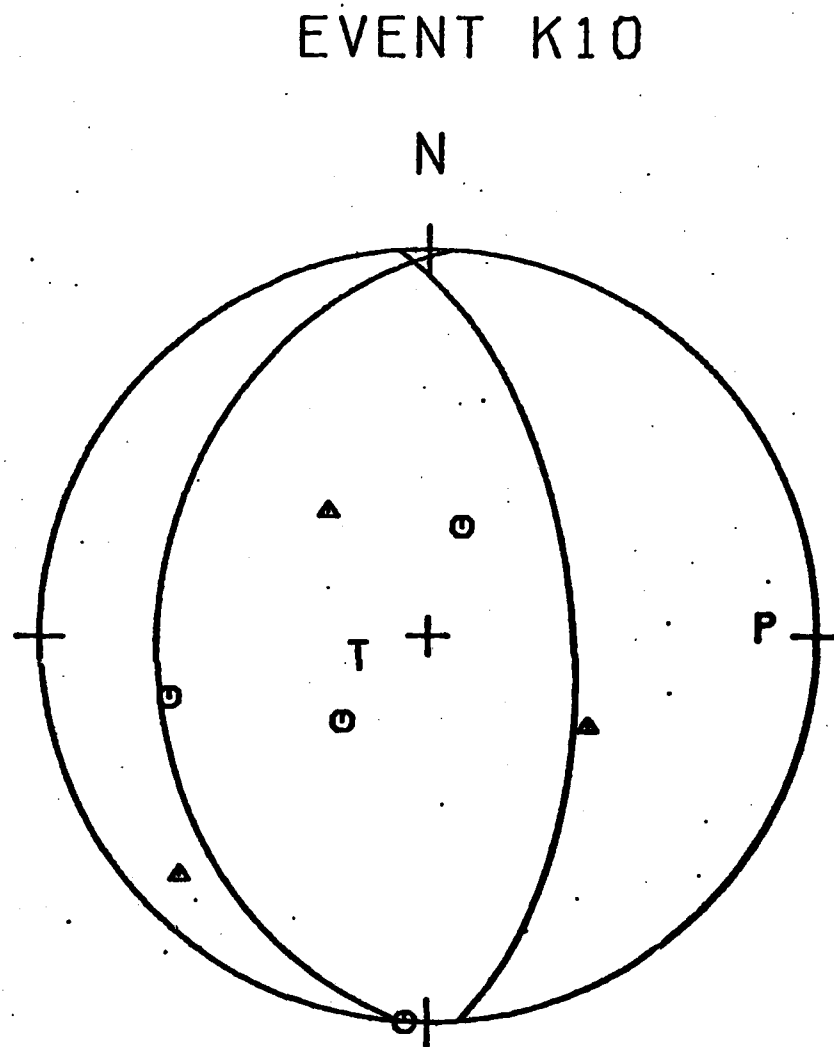


Figure 4j. Fault-plane solution for event K10 of the northwestern Kashmir mainshock-aftershock sequence.

EVENT K12

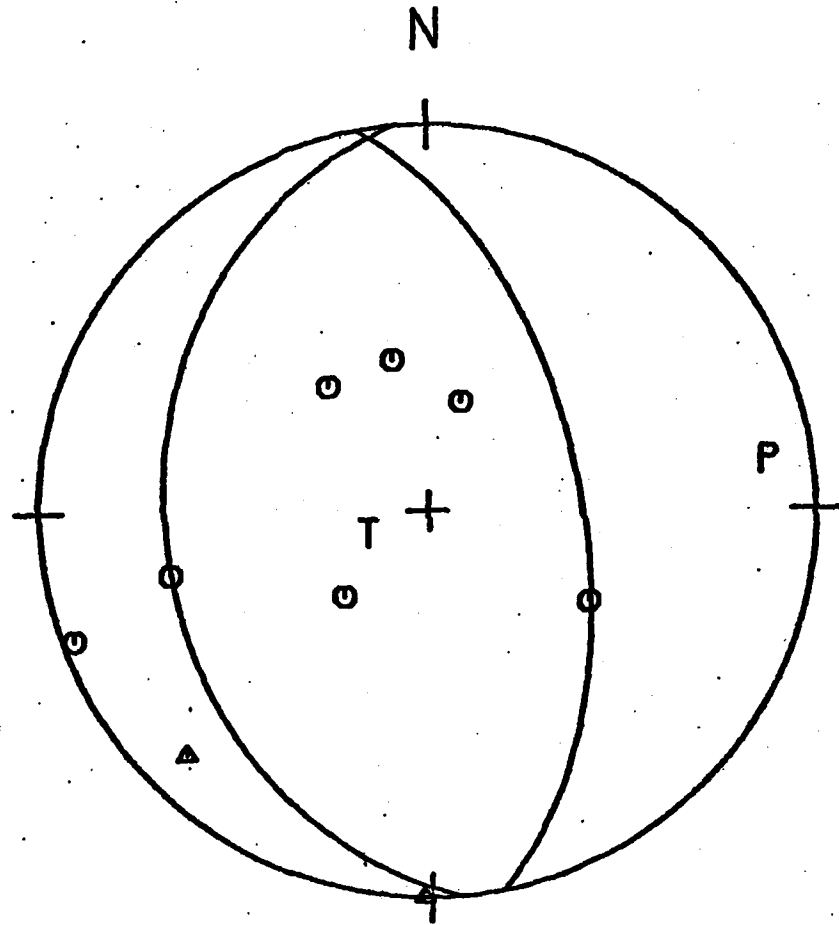


Figure 4k. Fault-plane solution for event K12 of the northwestern Kashmir mainshock-aftershock sequence.

EVENT K13

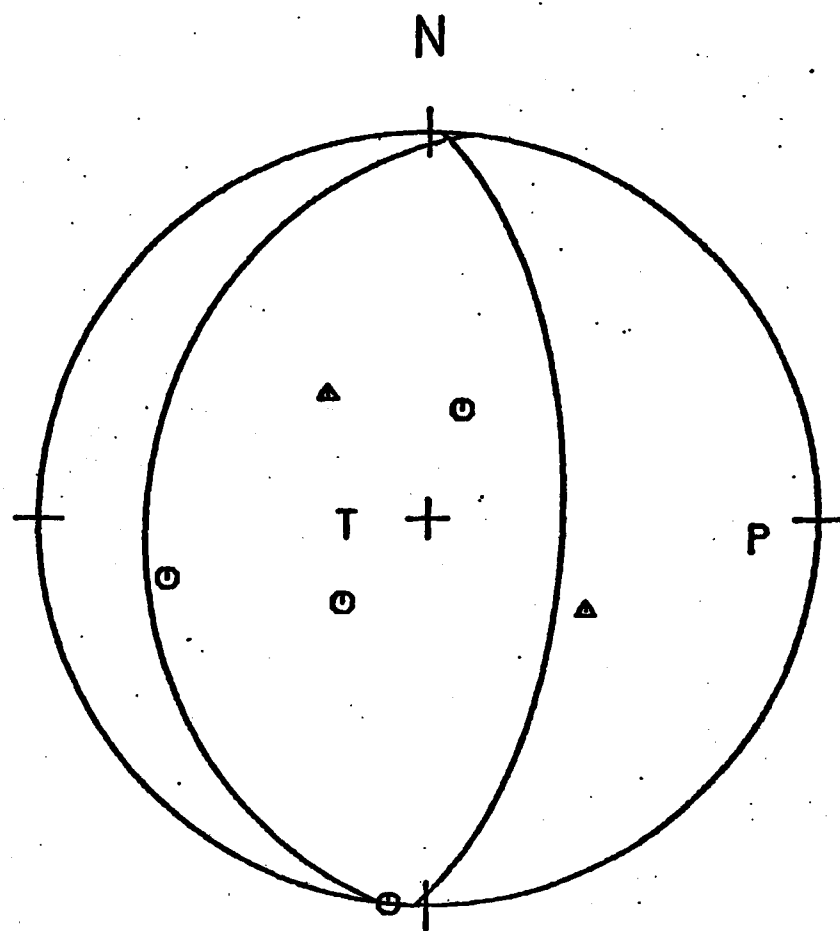


Figure 41. Fault-plane solution for event K13 of the northwestern Kashmir mainshock-aftershock sequence.

EVENT K14

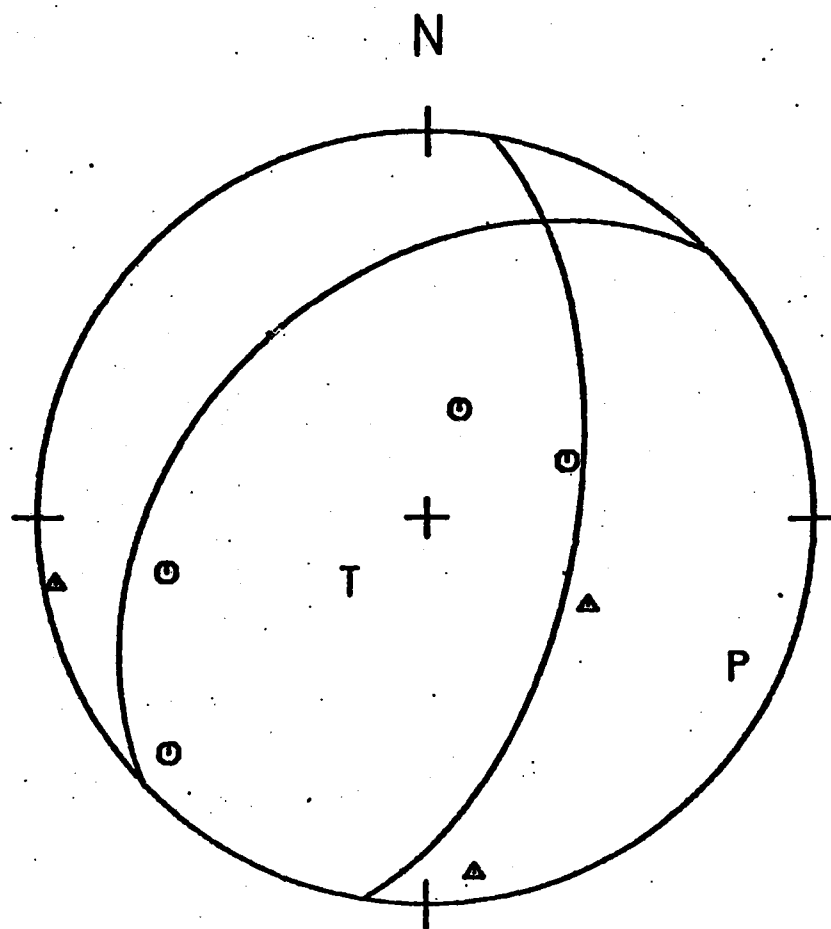


Figure 4m. Fault-plane solution for event K14 of the northwestern Kashmir mainshock-aftershock sequence.

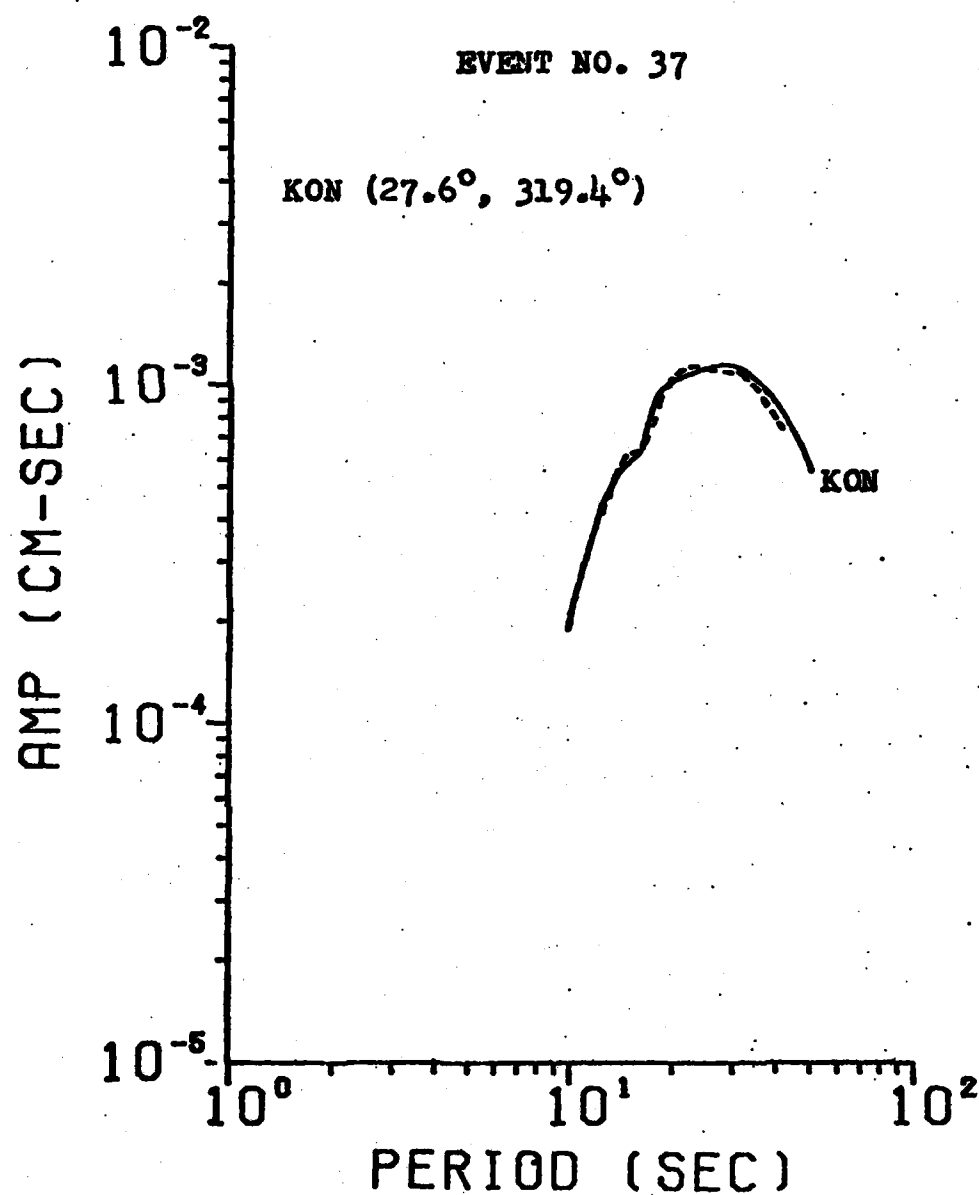


Figure 5a. Amplitude spectrum of fundamental-mode Love waves for event No. 37 recorded at VLPE station KON. The peak magnification for the high gain instrument (solid curve) is about 20 times that for the low gain instrument (dashed curve).

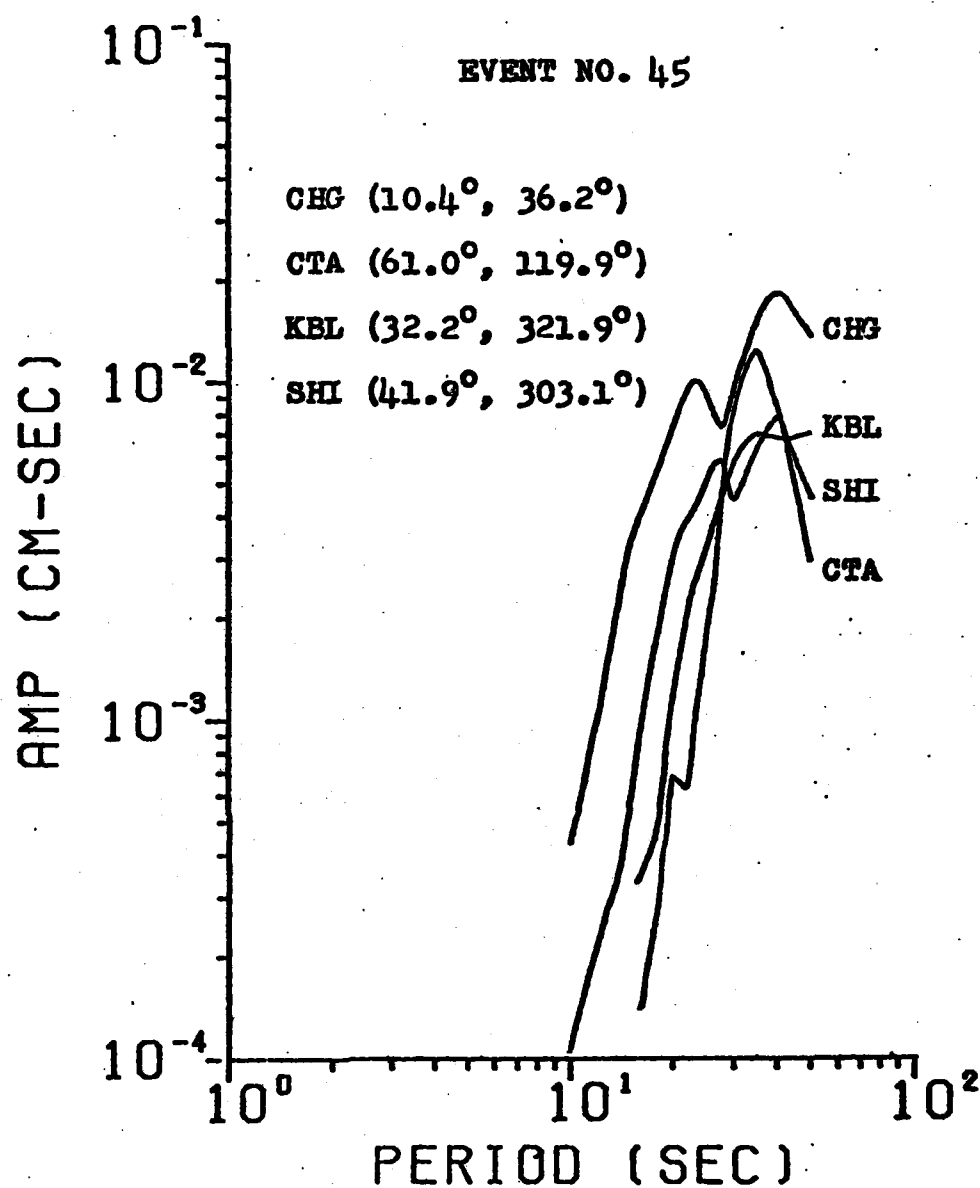


Figure 5b. Amplitude spectra of fundamental-mode Love waves for event No. 45.

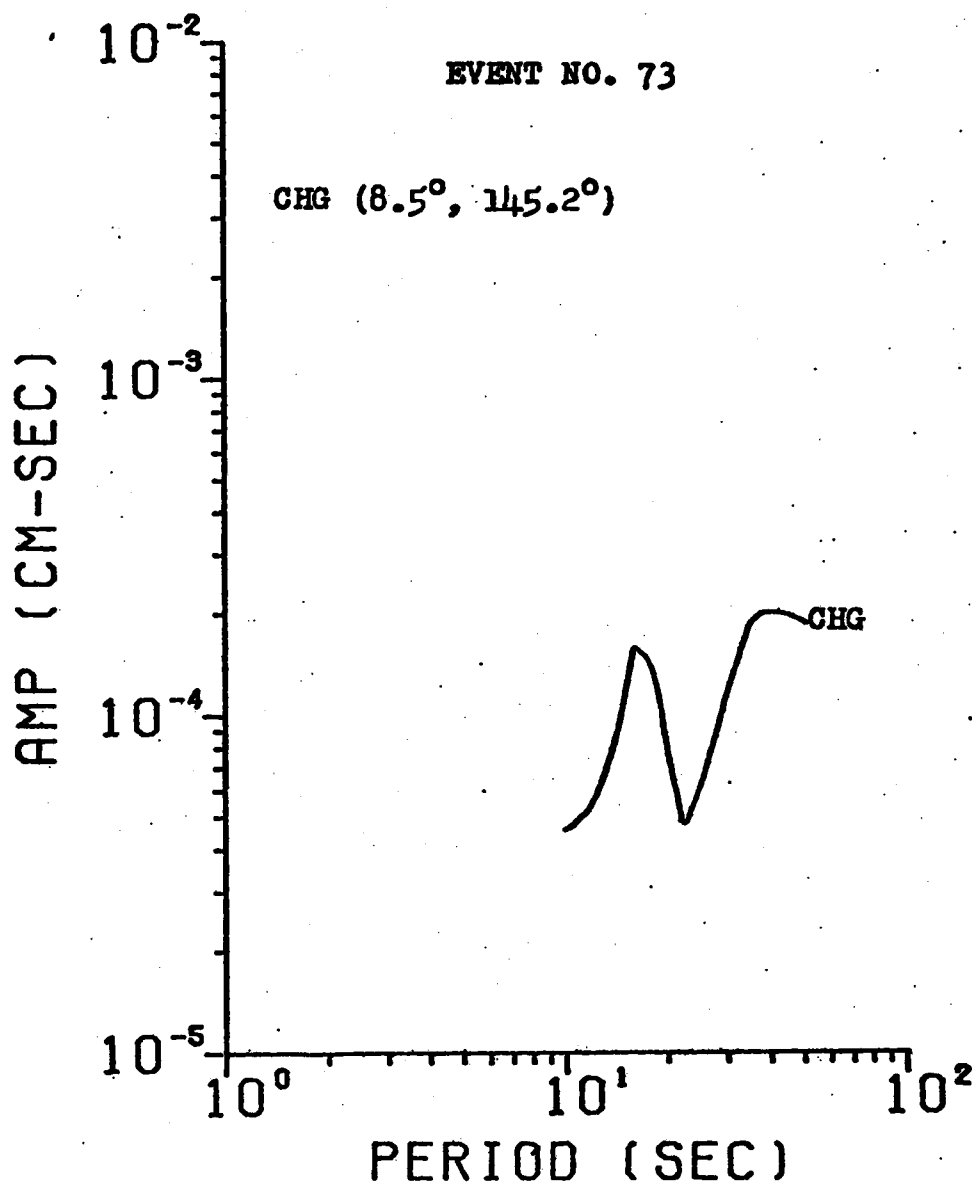


Figure 5c. Amplitude spectrum of fundamental-mode Love waves for event No. 73.

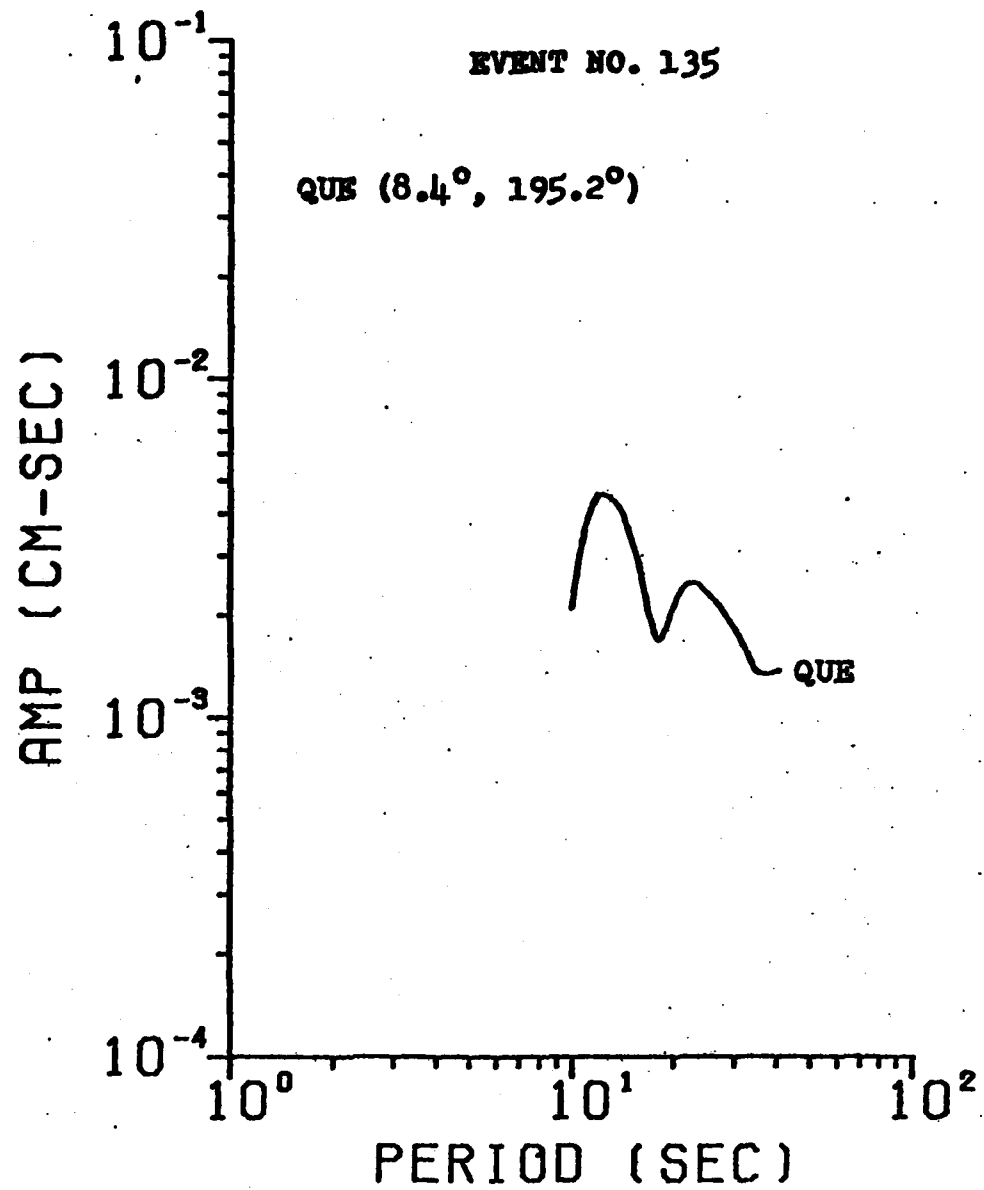


Figure 5d. Amplitude spectrum of fundamental-mode Love waves for event No. 135.

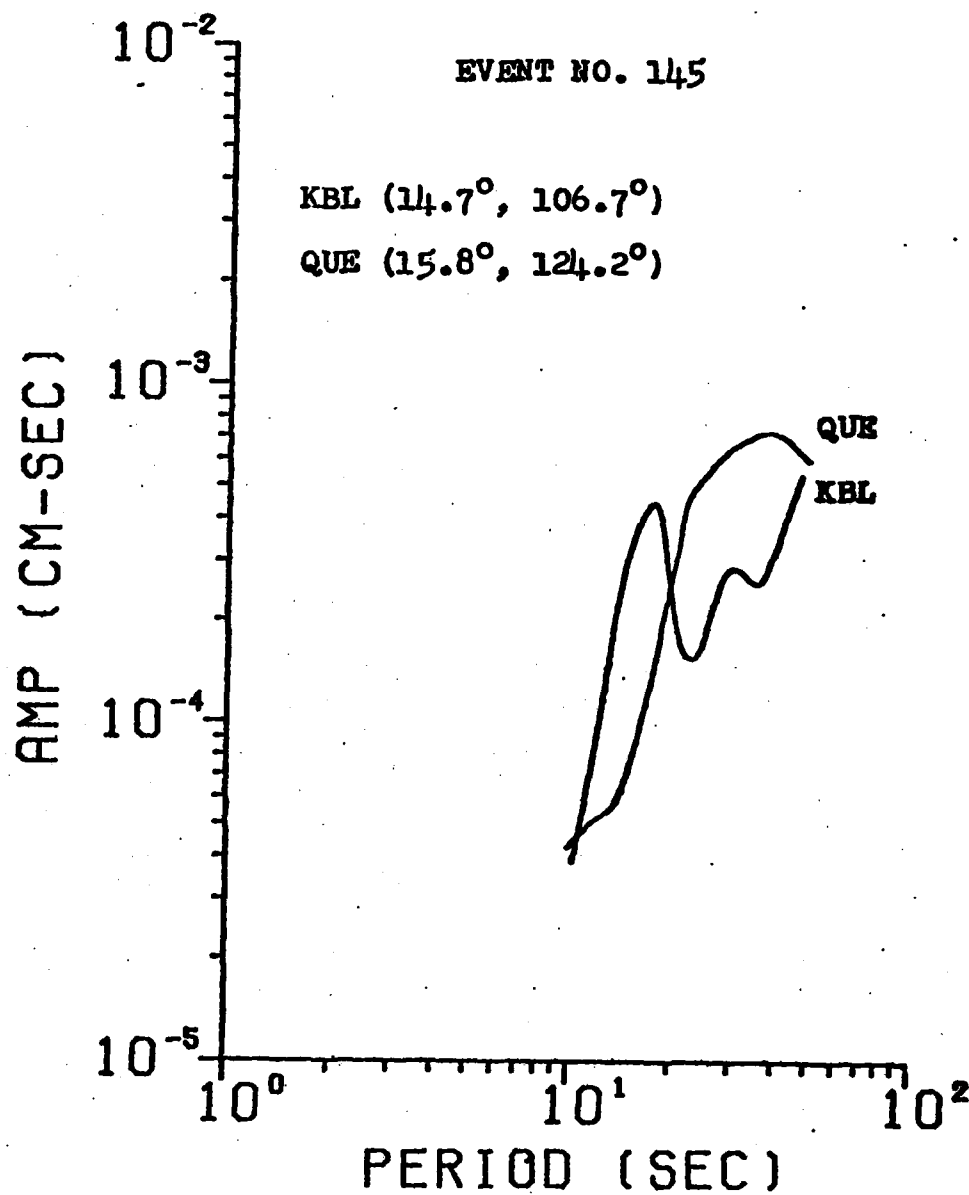


Figure 5e. Amplitude spectra of fundamental-mode Love waves for event No. 145.

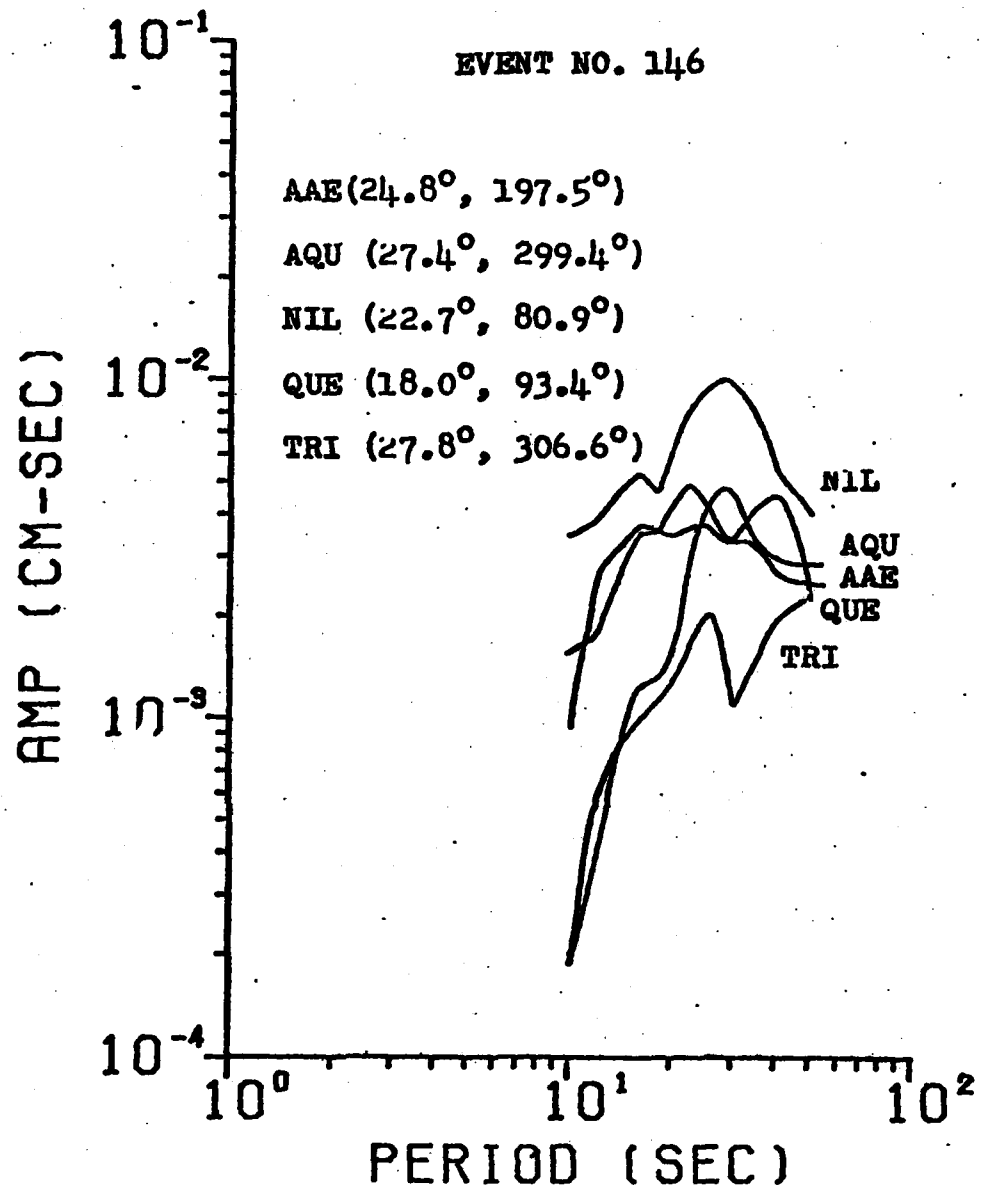


Figure 5f. Amplitude spectra of fundamental-mode Love waves for event No. 146.

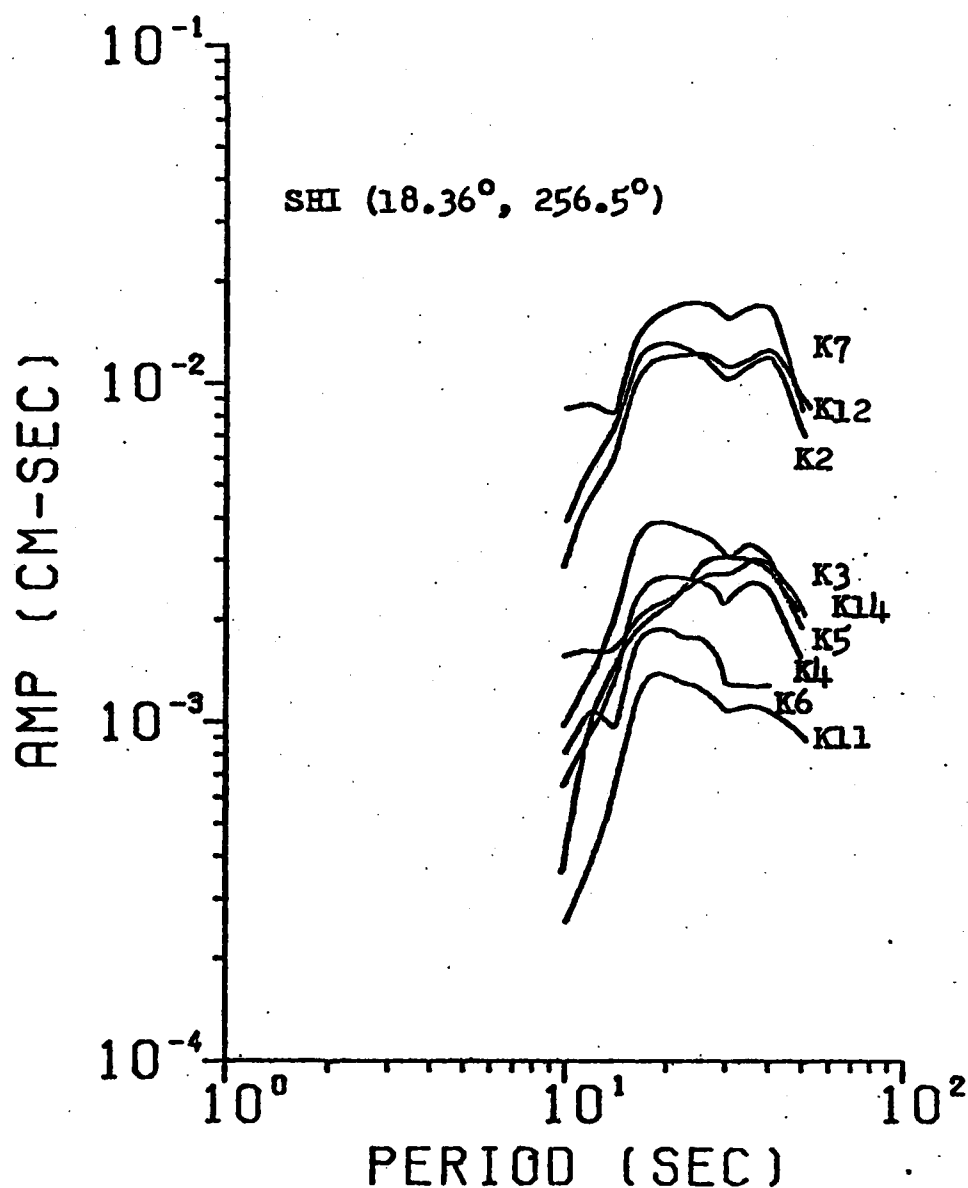


Figure 6a. Amplitude spectra of fundamental-mode Love waves for Kashmir earthquakes recorded at SHI (Shiraz, Iran). The numbers following the station code are epicentral distance and azimuth to the station. The character attached to each curve represents the particular Kashmir event.

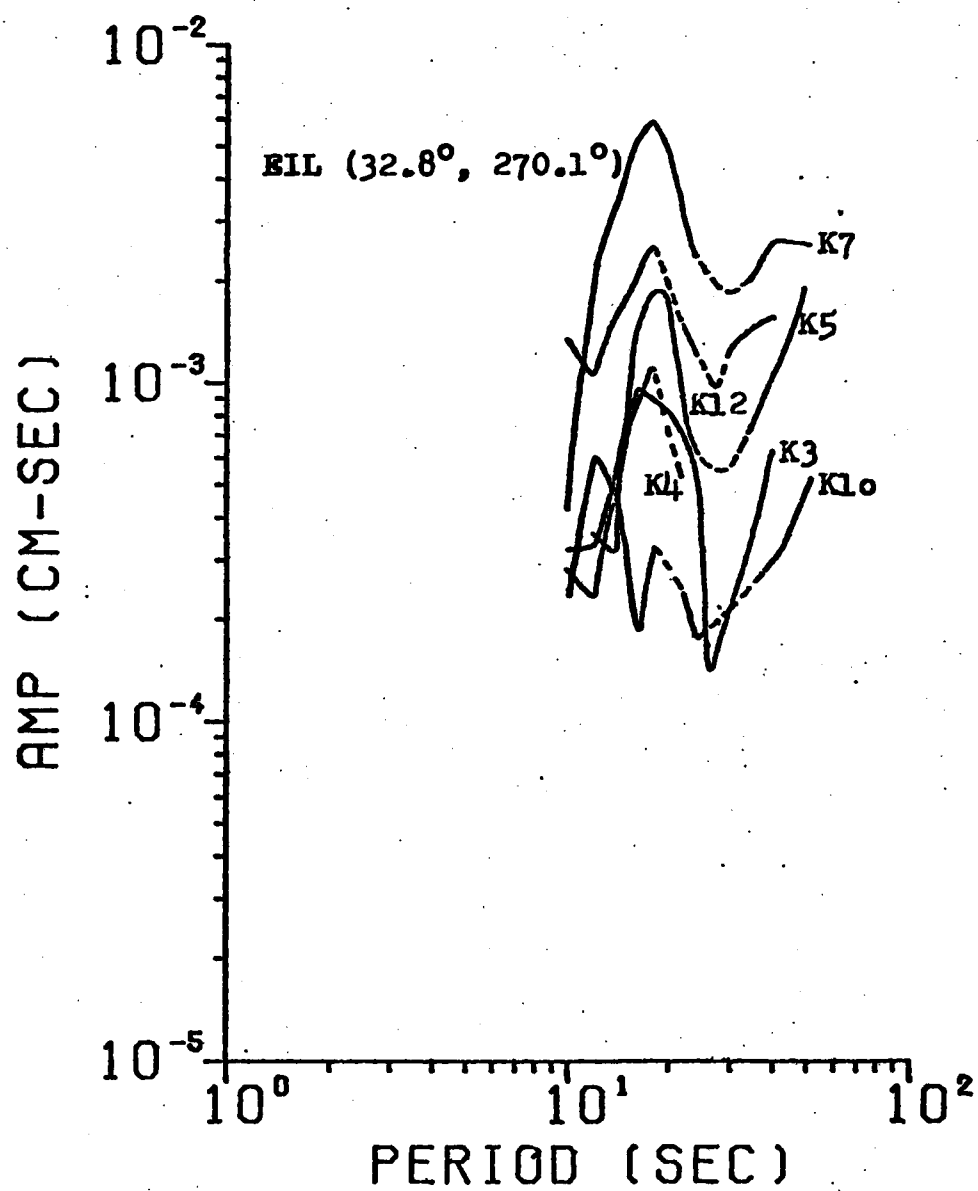


Figure 6b. Amplitude spectra of fundamental-mode Love waves for Kashmir earthquakes recorded at EIL (Eilat, Israel).

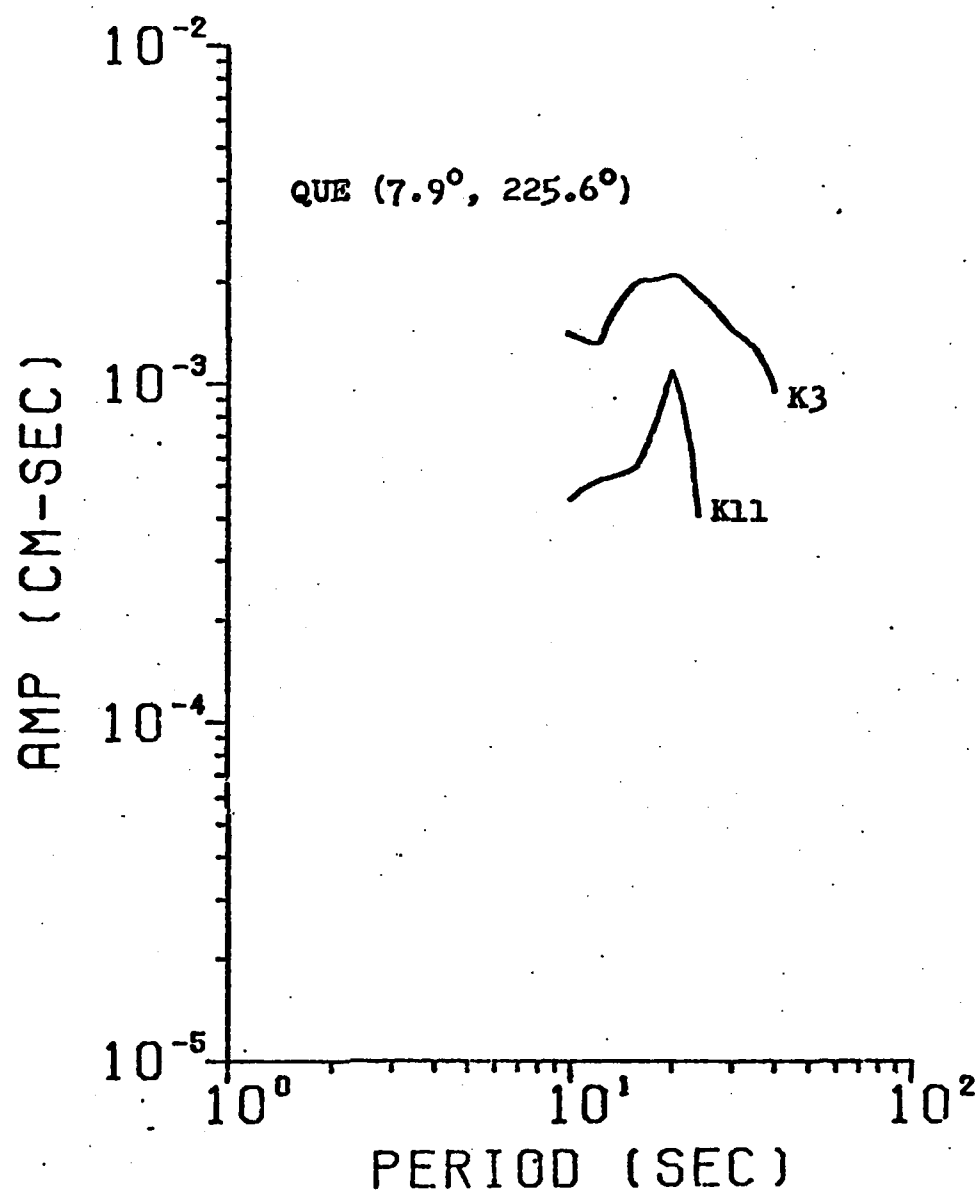


Figure 6c. Amplitude spectra of fundamental-mode Love waves for Kashmir earthquakes recorded at QUE (Quetta, Pakistan).

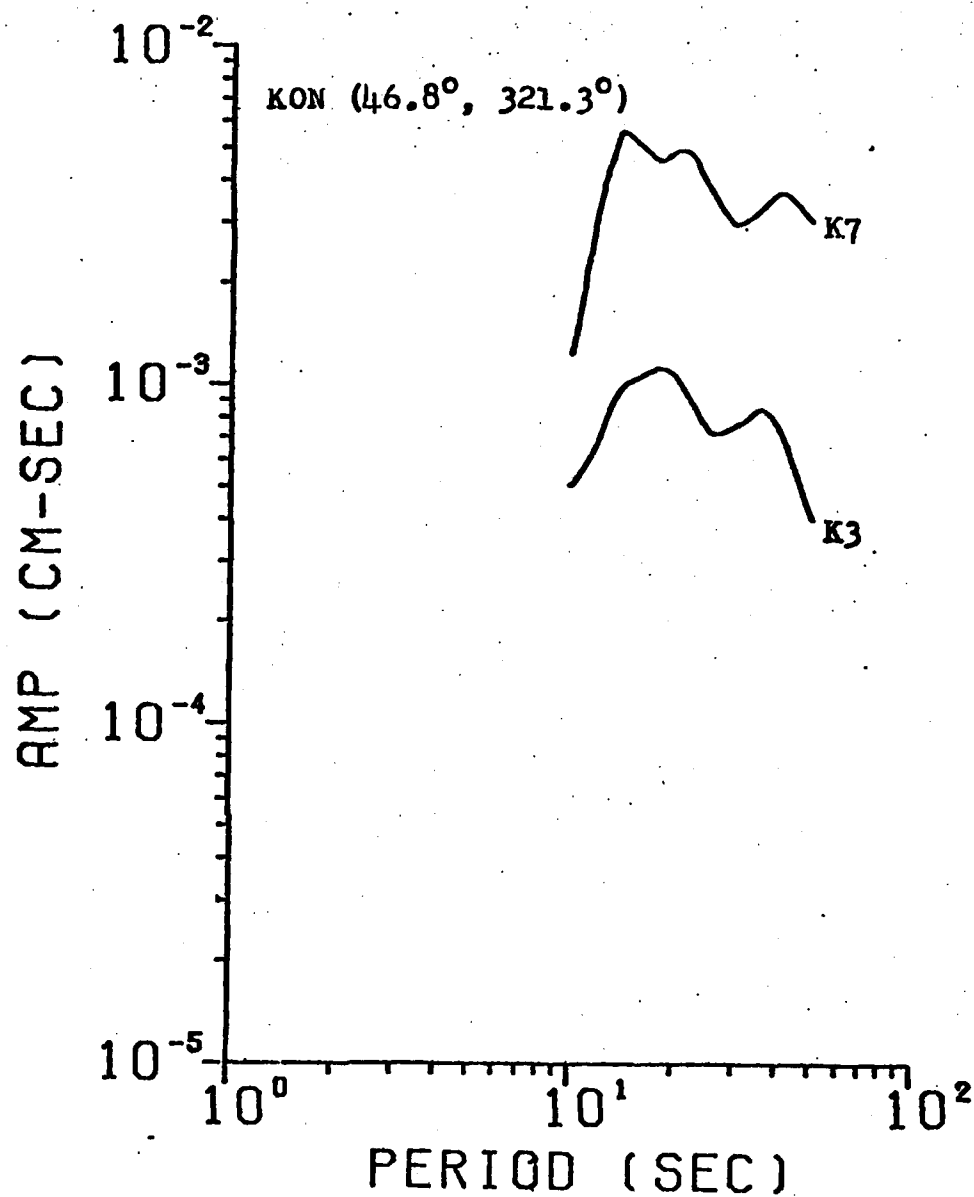


Figure 6d. Amplitude spectra of fundamental-mode Love waves for Kashmir earthquakes recorded at KON (Kongsberg, Norway).

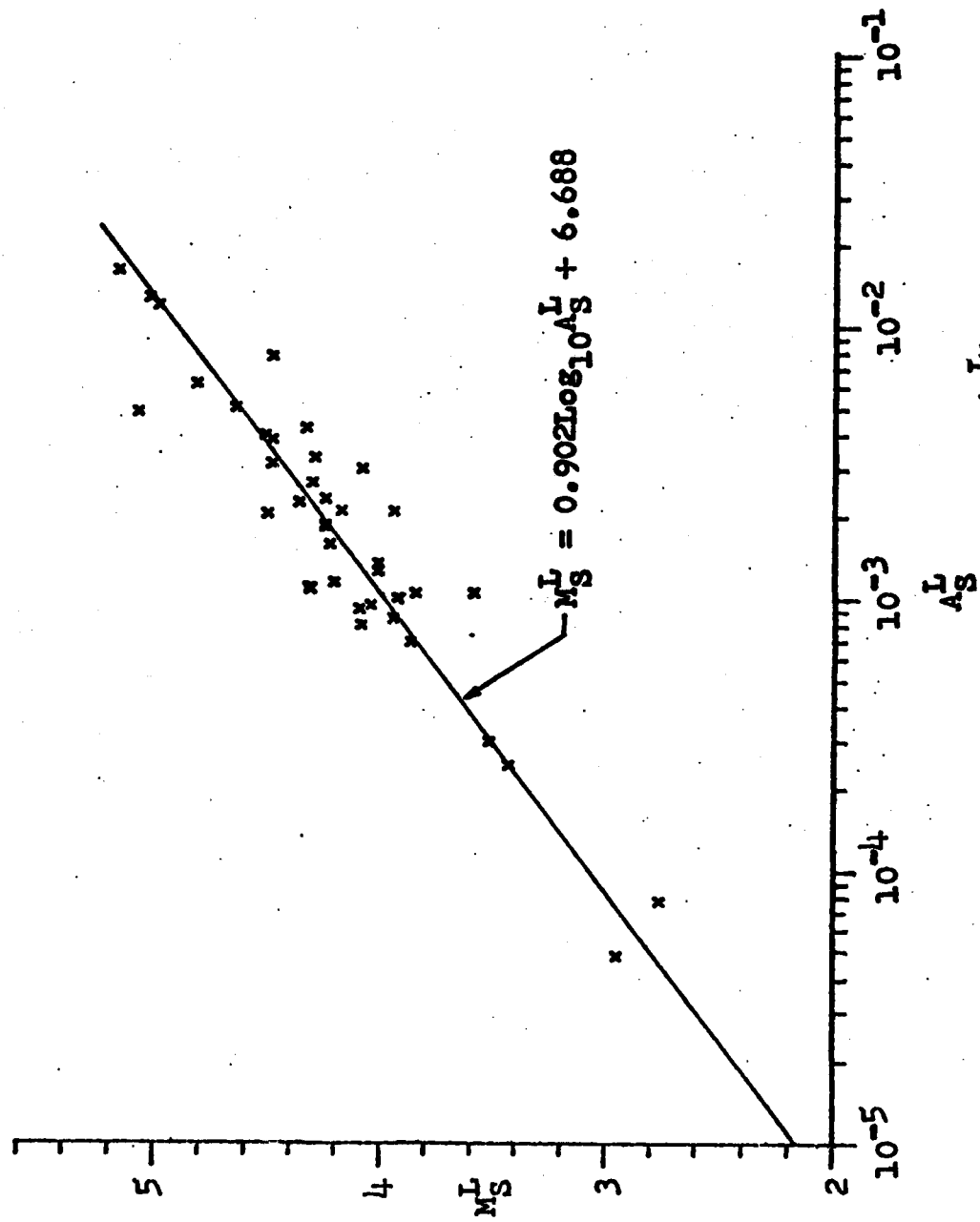


Figure 7. Relation between Love-wave magnitude (M_S^L) and spectral amplitude (A_S^L) at 20-sec period and at 9° epicentral distance. All the data from Table 3 and Table 5 are included in the figure.

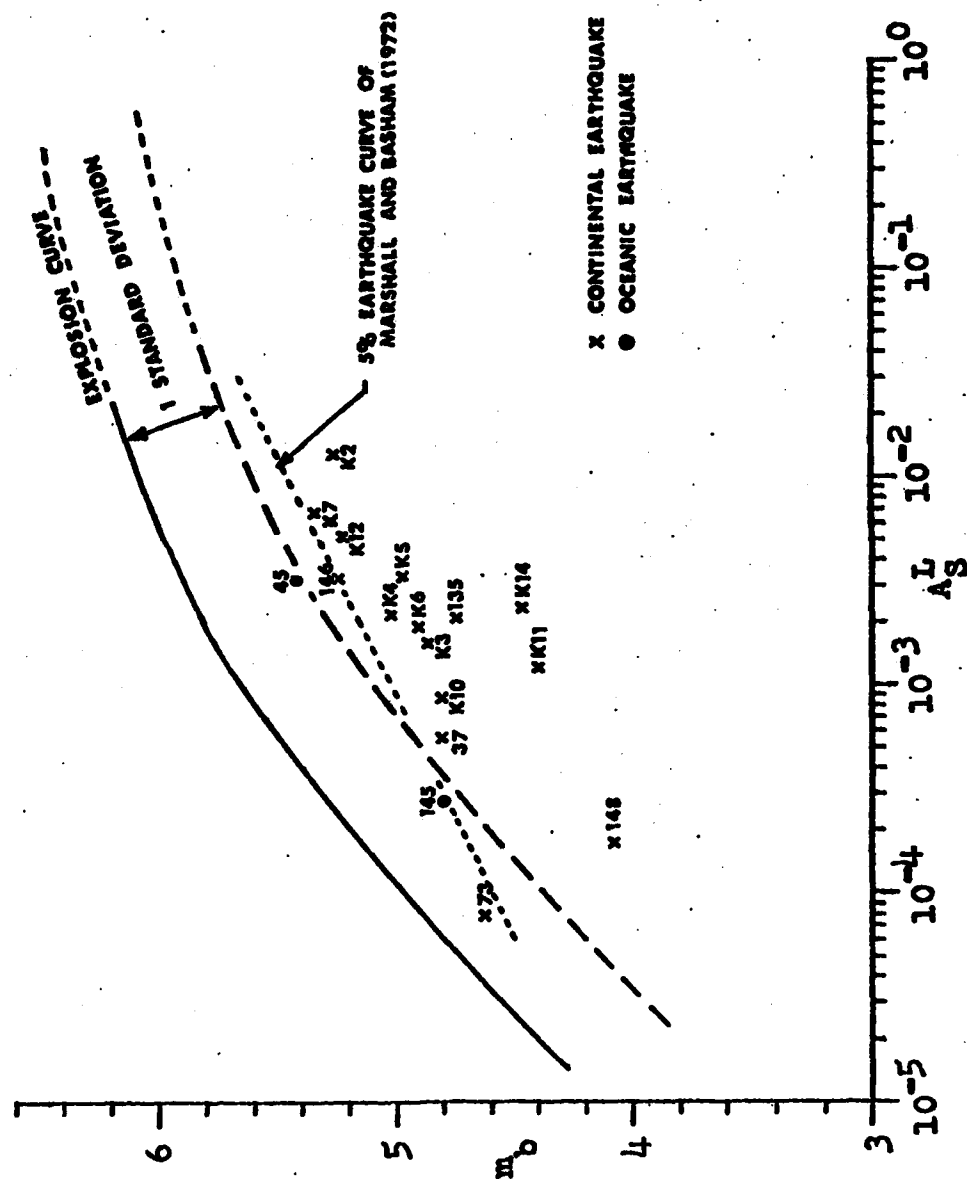


Figure 8 m_b versus A_S^L values for all the Eurasian events studied in this paper.

MODELLING COMPLEX EARTHQUAKES

by

Jaime Yamamoto

Introduction

It is well known among seismologists that seismograms from large shallow earthquakes very often have a complicated appearance near the beginning of the record. This complex appearance presents itself as small amplitude onsets prior to the P-wave arrival and sometimes as small glitches on the P-wave trace which noticeably distort its shape. The main characteristic of these onsets and glitches is that in general they cannot be associated with any known phase.

The complication in shallow focus earthquake records may be explained in at least four ways: (1) structure beneath the epicenter and/or interactions with the free surface, (2) earthquake multiplicity, (3) ray-path effects and (4) station effects.

The last two effects mentioned in the above paragraph can be diminished by studying records from stations at an appropriate range of epicentral distances (30° - 80°) and by observing only features that can be observed at several stations. Therefore, our main concern at this moment is to investigate whether the complication shown by some shallow focus earthquakes is produced by interaction with the structure in which the source is embedded or is a multiplicity effect.

Method of Analysis

The technique will be to match the observed long-period teleseismic P-wave signals with synthetic seismograms computed by the Haskell-Thomson

method. The program HASKELL written by Herrmann (unpublished, 1974) with slight modifications was used for the generation of the required synthetic seismograms. The theory used in writing this program is contained in Haskell (1964) and Hudson (1969) and an application appears in Herrmann (1976).

In this program the far-field source time function is represented by a trapezoid of area numerically equal to the seismic moment of the earthquake. The range of epicentral distances is restricted to 30-80° to avoid the complications produced by the heterogeneities of the upper-most mantle. The program options include source crust response, receiver crust response, anelastic attenuation, and instrument response.

Some Results

The method is being applied to several earthquakes which have occurred near the coast of Chiapas, Mexico. In this progress report I will present some preliminary results for two earthquakes that occurred in that area on April 29, 1970 at 11:22 GMT ($M_s = 6.3$) and April 30 at 08:33 ($M_s = 6.4$). The epicentral coordinates are 14.50N, 92.77W and 14.58N, 93.20W, for the first and second event respectively. Both earthquakes have almost the same depth of about 15 km based on pP - P readings. From P-wave first motion data (54 compressions and 1 dilatation), the two earthquakes show identical fault-plane solutions (strike = N92E, dip = 20°, slip = 71°). The mechanism represents reverse faulting. The spatial distribution of aftershocks was used as an aid in deciding which of two nodal planes correspond to the fault plane. It should be noticed that the nodal planes are not well constrained due to the fact that only one station recorded a dilatation. In future studies, I plan to use other methods in an attempt to improve the solution.

The two events are part of an earthquake sequence that took place about 100 km off the coast of Chiapas, Mexico in April, 1970. They were chosen because they show similarities in magnitude, location and source geometry, but at the same time the appearance of the long-period P-wave signals are quite different (see Figures 1 and 2).

The shape of the P-wave for the earthquake which occurred at 08:33 as observed at the station BKS (distance = 35 degrees, azimuth = 317 degrees) looks very simple suggesting a simple rupture process. The synthetic seismogram displayed on the same figure was computed assuming as a source function an isosceles triangle with a base of 5 seconds and an area arbitrarily taken equal to 10^{25} . The velocity structure at the source region was obtained from extensive refraction studies carried out in that area (Shor and Fisher, 1961). The structure beneath the recording station was assumed to be a simple two-layer crust typical of continental regions.

The agreement between the synthetic and observed seismograms in Figure 1 is quite good for the first 30 seconds. For later times the seismogram is largely controlled by reflections and conversions coming from deep interfaces. At these depths (about 200 km) the velocity model is not known very well.

The observed record of the 11:22 earthquake exhibits a far more complicated character (see Figure 2). It shows an extra secondary arrival superimposed on the first down swing. The amplitude of the second upswing has been severely attenuated. The relative amplitude of a third upswing has, on the other hand, increased. The features are common to most of the stations.

A set of synthetic seismograms were generated assuming a simple source time function located at various depths. None of these synthetics look like the observed seismogram. Therefore, we have to resort to

multiple events in order to explain the observed complexities. A source function composed of two isosceles triangles of base equal to 5 seconds and separation between peaks equal to 5 seconds was used to simulate two consecutive events. The seismic moment of the second event was chosen to be two times larger. The synthetic and observed seismograms are shown on Figure 2. The first 13 seconds of seismogram agree reasonably well. An extra second arrival approximately 5 seconds after the first P arrival is clearly shown by the synthetic. For greater times, there is a considerable discrepancy between the theoretical and observed signals. In particular, a large second upswing is predicted, but is not seen on the real seismogram. The computed third upswing, on the other hand, is small as compared with that of the observed record. At this time, the reasons for the discrepancy are not known. The rupture process of this earthquake is likely to be more complicated than assumed, therefore the simple superposition of two sources may not work properly. Further work will concentrate on using more complex source models.

References

- Haskell, N.A. (1964). Radiation patterns of surface waves from point sources in a multi-layered medium, Bull. Seism. Soc. Am., 54, 377-393.
- Herrmann, R.B. (1976). Focal depth determinations from the signal character of long-period P waves, Bull. Seism. Soc. Am., 66, 1221-1232.
- Hudson, J.A. (1969). A quantitative evaluation of seismic signals at teleseismic distances, II. Body waves and surface waves from an extended source, Geophys. J. Roy. Ast. Soc., 18, 353-370.
- Shor, G.C., and R.L. Fisher (1961). Middle America trench. Seismic refraction studies, Geol. Soc. Am. Bull., 72, 721-730.

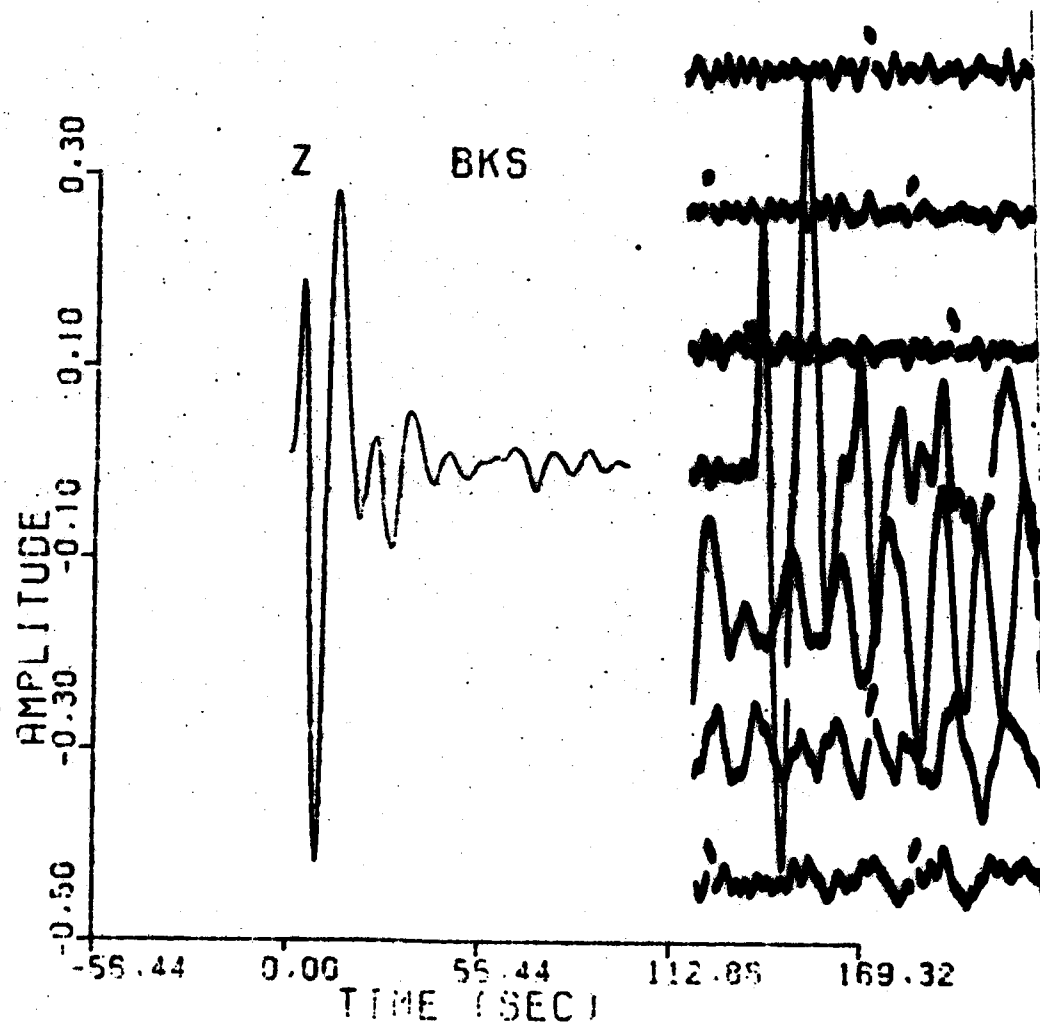


Figure 1. Synthetic (left) and observed (right) P-wave signals at BKS (distance = 35° and azimuth = 317°) for the April 30, 1970 event. Synthetic was computed for a source depth of 15 km. The amplitude units are arbitrary.

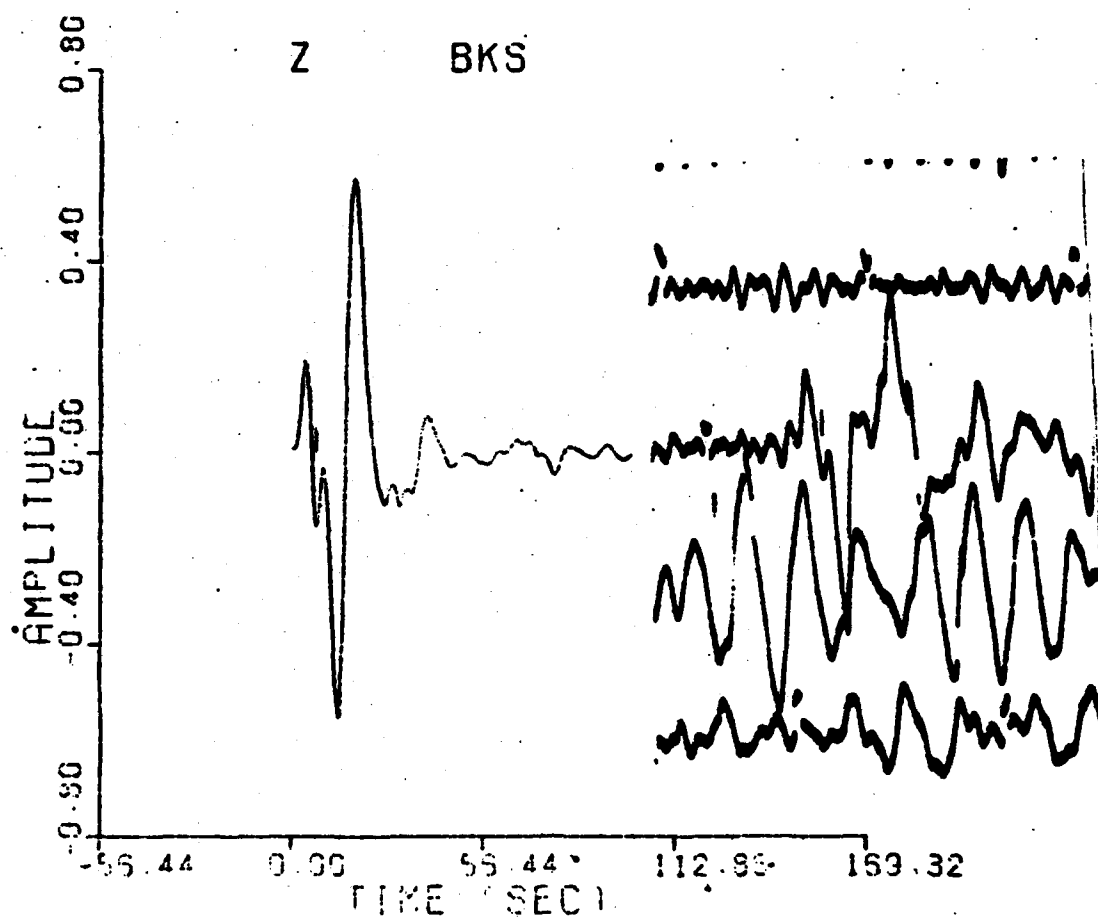


Figure 2. Synthetic (left) and observed (right) P-wave signals at BKS for the April 29, 1970 event. Synthetic computed for a source depth of 15 km. The amplitude units are arbitrary.

THE EFFECT OF COMPLEX NEAR-SOURCE CRUSTAL STRUCTURE
ON THE WAVE FORMS OF RAYLEIGH WAVES

by

Brian J. Mitchell and Chiung-Chuan Cheng

An extensive study of the attenuation of Rayleigh wave spectral amplitudes across Eurasia has been reported by Yacoub and Mitchell (1977). The confidence limits of their observed Rayleigh wave attenuation coefficients were substantially larger than confidence limits for attenuation coefficients in North America (Herrmann and Mitchell, 1975). The large confidence limits for the Eurasian data probably reflect the complex structure across which most of the Rayleigh waves passed. Lateral refraction and multi-pathing which originate along the propagation paths of the Rayleigh waves are obvious possibilities as causes of scatter in the data. Another possibility is that lateral complexities in the source region perturb the Rayleigh waves as they are being formed. The purpose of the present research is to investigate the extent to which near-source complexities affect the wave forms of fundamental mode Rayleigh waves observed at distant stations in Eurasia.

Methodology

The effects of near-source structure and multi-pathing on the wave forms of Rayleigh waves can be studied by comparing the observed wave forms with synthetic Rayleigh wave seismograms. Dr. R.B. Herrmann has written a program for such computations which he has permitted us to use for this study. Necessary input for theoretical seismogram calculations are the following: (1) the fault-plane solution for the earthquake which produced

the Rayleigh waves being studied, (2) the amplitude spectrum at the source, (3) attenuation coefficient values as a function of period for each mode, and (4) a knowledge of the instrument response for the seismographs used.

Fault-plane solutions for these computations are available for three of the earthquakes studied by Yacoub and Mitchell (1977). Two of these have been used as sources for synthetic seismogram computations in this study. In addition, synthetic seismograms were computed for a nuclear event at Novaya Zemlya. The source spectrum was estimated from the magnitudes of the events and the scaling relationships of Aki (1967). Attenuation coefficients corresponding to shield regions for fundamental and higher modes have been computed by Mitchell et al (1977) and were used for all computations in this study. Instrument responses were computed for the long-period WSSN instruments used for this research. Seven modes were used for all of the computations in this work. These were computed for the Baltic shield model of Nojonen et al (1967).

Results

The synthetic seismograms calculated as described above were compared to observed seismograms for selected events and stations. Figure 1 (from Yacoub and Mitchell, 1977) is a map of the events and stations for which observed Rayleigh wave seismograms are available. Synthetic seismograms were first computed for events near a transition between stable and tectonic regions, and for paths which were entirely across stable regions. The earthquakes with known fault-plane solutions which occurred near such a transition are those of October 28, 1971 and November 18, 1971. Stations to which paths were restricted to stable regions are those in northern Europe. Results of the first computations appear in Figures 2 and 3. The agreement between the main features of the observed and theoretical seismograms is

is good. The durations and shapes of the envelope of the observed wave forms are similar to those for the computed wave forms in all cases except that of the November 18 event as recorded at NUR. The duration of the envelope of the first 100 seconds is, however, very similar to that of the synthetic seismogram. Later energy bursts appear on the observed seismogram which are not predicted theoretically. These cannot be caused by near-source complexities since they are so much later than the first energy group; they may be due to multi-pathing which arises along the propagation paths. Although near-source complexities, for the above examples, do not have a large effect on the gross features of the wave forms studied, they may have a perturbing effect which is difficult to separate from other effects, such as multi-pathing or departures of fault-motion from that of the idealized sources which are assumed for the synthetic seismogram computations.

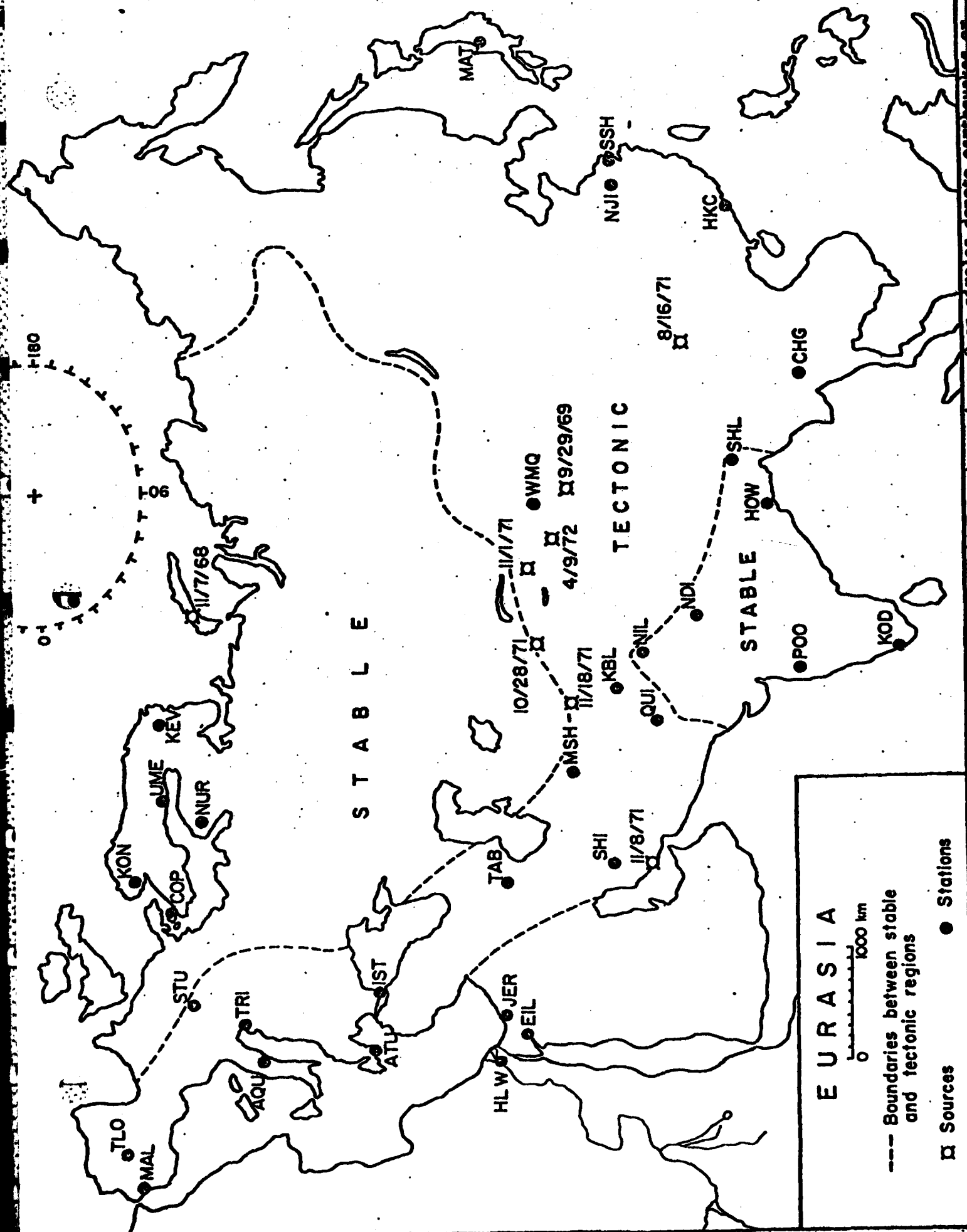
A Novaya Zemlya nuclear event (November 7, 1968) was studied as an example of a source near a continental boundary. Synthetic seismograms were computed in the same way that they were for earthquakes, except that the source radiation pattern was taken to be circular and the source spectrum included a peak such as that which appears in published source spectra of nuclear explosions (e.g. von Seggern and Lambert (1970)).

Observed and theoretical Rayleigh waves from the Novaya Zemlya event of November 7, 1968 to stations MSH and KBL appear in Figure 4. The observed seismograms differ substantially from the theoretically predicted seismograms in all cases. The reason for the differences cannot as yet be ascertained. Possible reasons for the differences include the effect of lateral complexities near the source, the presence of a water layer near the source, or departures of the source spectrum from that which was assumed.

Rayleigh waves for paths across the tectonic regions of Figure 1 differ greatly from those which cross the stable regions (see Figure 5). Different sub-regions within the broad region designated as tectonic also produce seismograms which differ considerably from one another. For instance, the seismogram recorded at a station in the Mediterranean region (AQU) has a very poorly developed Rayleigh wave which appears to be dominated by multi-pathing. The other two stations (MSH and SHL) in central Asia have well-dispersed wave trains which differ greatly from those recorded for shield paths. Further synthetic seismogram computations are in progress for models corresponding to the tectonic regions of Eurasia. These should tell us if the features of the observed seismograms are produced by the velocity structure in the region, or if multi-pathing or near-source complexity are important.

References

- Aki, K. (1967). Scaling law of seismic spectrum, J. Geophys. Res., **72**, 1217-1231.
- Herrmann, R.B., and B.J. Mitchell (1975). Statistical analysis and interpretation of surface-wave anelastic attenuation data for the stable interior of North America, Bull. Seism. Soc. Am., **65**, 1115-1128.
- Mitchell, B.J., N.K. Yacoub, and A. Correig (1977). A summary of observed surface wave attenuation and its regional variation across continents and oceans, Am. Geophys. Union Mono. **20**, in press.
- Nojonen, I., M.T. Porkka, S. Pirhonen and U. Luosto (1967). The crust and mantle in Finland, J. Phys. Earth, **15**, 19-24.
- Seggern, D. von, and D.C. Lambert (1970). Theoretical and observed Rayleigh-wave spectra for explosions and earthquakes, J. Geophys. Res., **75**, 7382-7402.
- Yacoub, N.K., and B. J. Mitchell (1977). Attenuation of Rayleigh-wave amplitudes across Eurasia, Bull. Seism. Soc. Am., in press.



October 28, 1971

KEV - obs



KEV - th



NUR - obs



NUR - th



Figure 2. Observed and synthetic Rayleigh wave seismograms for the USSR earthquake of October 28, 1971. The Rayleigh waves travelled almost entirely across stable regions to stations KEV and NUR. The time scales indicate the duration of the plotted trace in minutes.

November 18, 1971

KEV - obs



KEV - th



NUR - obs



NUR - th

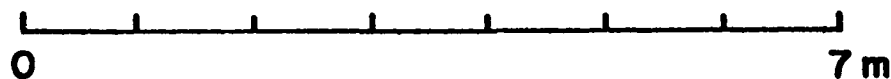


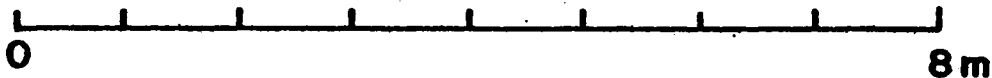
Figure 3. Observed and synthetic Rayleigh wave seismograms for the USSR earthquake of November 18, 1971. The Rayleigh waves travelled almost entirely across stable regions to stations KEV and NUR. The time scales indicate the duration of the plotted trace in minutes.

November 7, 1968

MSH - obs



MSH - th



KBL - obs



KBL - th



Figure 4. Observed and synthetic Rayleigh wave seismograms for the Novaya Zemlya nuclear event of November 7, 1968. The Rayleigh waves travelled almost entirely across stable regions to stations MSH and KBL. The time scales indicate the duration of the plotted trace in minutes.

November 18, 1971

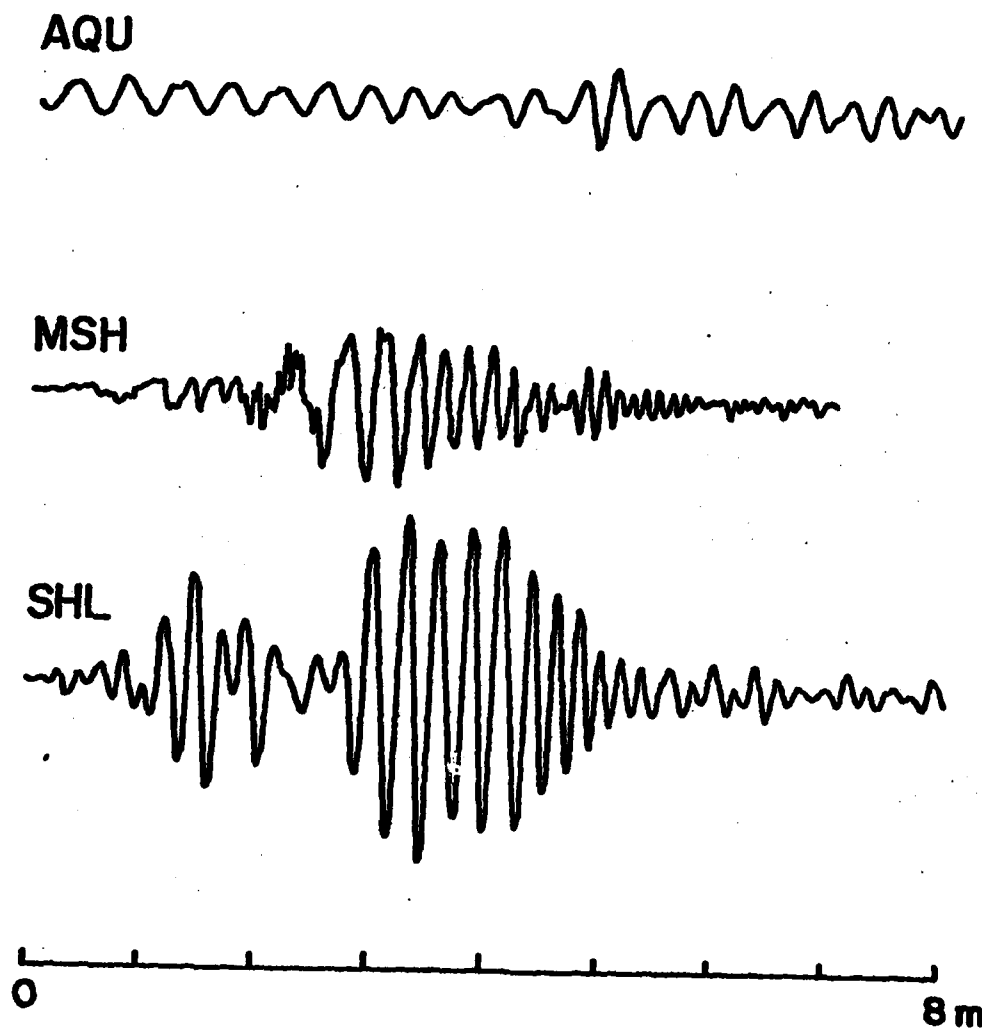


Figure 5. Observed seismograms from the USSR earthquake of November 18, 1971. The Rayleigh waves travelled along complex tectonic paths to the stations AQU, MSH, and SHL. The time scales indicate the duration of the plotted trace in minutes.